BIDIRECTIONAL CARGO TRANSPORT BY MICROTUBULE-BASED MOLECULAR MOTORS

BY

MELINDA TONKS HOFFMAN

DISSERTATION

Submitted in partial fulfillment of the requirements
for the degree of Doctor of Philosophy in Physics
in the Graduate College of the
University of Illinois at Urbana-Champaign, 2011

Urbana, Illinois

Doctoral Committee:

Assistant Professor Yann Chemla, Chair
Professor Paul Selvin, Director of Research
Assistant Professor Aleksei Aksimentiev
Professor Russell Gianetta

Abstract

We have reconstituted a simple *in vitro* system using only mammalian dynein and mammalian kinesin attached to a single cargo. These cargoes undergo saltatory motion typically seen *in vivo*, indicating that the motors engage in a tug-of-war. When the complex hits a barrier, the cargo often reverses direction. In some cases, it tries several up-and-back motions, during which time the dynein likely pulls the cargo onto a different protofilament, and is sometimes able to bypass the blockage. This explains why eliminating kinesin or dynein stops motion in both directions *in vivo*. We also find that mammalian dynein, but not kinesin, often takes backwards steps when under backward force. However, yeast dynein coupled with mammalian kinesin does not display these attributes, as expected.

Acknowledgements

To Kevin, for hundreds of 100 mile trips to and from Purdue so that I could stay here and get a Ph.D, not to mention all the love and support and doing of dishes.

And to my dad, for teaching me to love learning and for informing me how silly it was to think I could be successful in graduate school without knowing how to program first.

To my mom, for her infinite depth of love and constant support.

And to my unborn child, for lighting a fire of urgency under my feet.

Contents

Chapter 1: Introduction and Background

Section 1.1 Overview

All cells have the need to transport various cargoes from one place inside the cell to another. In the small and simple prokaryotic cell, this is accomplished by means of simple diffusion. Proteins or other cell components are created in one location and are allowed to simply disperse by random diffusion until they reach their intended destination. The timescale required for this to occur can be estimated by using the mean square displacement for 3D diffusion: $<x^2>=6Dt$. The diffusion coefficient (D) has been measured for a small protein in a bacterial cell to be ~6 μm^2/sec*(1, 2)*. For a cell of about 2 μm in size, the time to diffuse this distance would be ~120 msec, which is on the order of the response time for bacteria to external stimuli*(1)*.

However, eukaryotic cells are not only vastly more complex than prokaryotic cells, but are much larger in size—on the order of 10-100 μm as compared to the prokaryote's ~1-5 μm (see Figure 1). In the larger, complex, and crowded eukaryotic cell, this increased distance between and complexity of various organelles within the cell means that diffusion simply takes too long to transverse the cell's volume. For example, if we assume a 50 μm diameter cell and a diffusion coefficient of 6 μm^2/sec, the time scale for a particle to diffuse this distance is ~70 seconds. This is far greater than the timescale necessary for the cell to perform its functions and respond to stimuli. The actual time required could even be far greater than this, in fact, as the diffusion coefficient inside the more crowded and complex eukaryotic cell would likely be lower than that predicted for a less crowded environment. In addition, the complex organization of the eukaryotic cell

organelles requires a more specific and directed approach to intracellular transport. Therefore, eukaryotic cells require a different mechanism by which to transport proteins and other cargoes from one place to another within the cell.

Molecular motors fulfill this capacity within eukaryotic cells. Molecular motors are a type of protein that can bind to a cargo and carry that cargo along as they "walk" from one point to another along certain "roadways" found within the cell. There are three main types of roadways found in cells, each of which is a part of the cell's structural cytoskeleton: actin, intermediate filaments, and microtubules. Figure 2 illustrates one of these three cytoskeleton components—the microtubule network. The image shows a cell with microtubules stained in green and the nucleus stained in blue.

On the microtubule network, there are two main types of motors which carry cargo: kinesin and dynein. In general, kinesin carries cargos from the nucleus to the outside of the cell (the + direction), while dynein carries cargos primarily from the cell membrane back into the nucleus (the – direction). Disruptions in organelle transport due to impaired motor function can cause great harm to the cell and contribute to neuronal disorders such as human peripheral neuropathy and Alzheimer's disease*(3)*.

Transporting a cargo to a desired location within the cell may seem a simple problem of attaching the appropriate motor and allowing it to walk in the motor's preferred direction until it reaches its destination. However, in living cells, both kinesin and dynein are attached to the same cargo, and these cargos are observed to constantly switch directions,

moving successively in the + and – directions with numerous pauses and direction reversals—a phenomenon known as saltatory motion. It is as yet unknown whether there is some external signal that mediates the cooperation of dynein and kinesin (turning one off and the other on such that both are not simultaneously pulling on the cargo), or if the mechanism governing saltatory motion is a simple tug-of-war between the two motors. The main objective of this dissertation will be to answer this question and to examine the interaction between dynein and kinesin attached to a single cargo.

Section 1.2 Microtubules

Microtubules are part of the cell's cytoskeleton, providing not only structural support but a roadway for molecular motors to walk upon. Microtubules have a structure like that of long "ropes" of about 25 nm in width and up to 25 μm in length, and are composed of bundles of protofilament "threads," generally with 13 protofilments per microtubule (see Figure 3). Each protofilament is in turn made up of polymerized tubulin subunits. The tubulin subunit is a dimer made up of an alpha subunit and a beta subunit. The protofilaments bundle together to form a hollow cylindrical unit with a helical pitch of approximately 13 tubulin dimers. The subunits are oriented in such a way that the microtubule has a distinct polarity, with a "+" end (which has the alpha subunit exposed) and a "-" end (which has the beta subunit exposed). Microtubules are highly dynamic inside a living cell, continually polymerizing and depolymerizing. The + end is the main site at which monomers are added as the microtubule polymerizes. In addition, microtubules are generally oriented radially outward from the center of the cell, with the + end pointing towards cell periphery, and the – end near the nucleus.

In the cell, microtubules have many different types of protein bound to them in addition to motor proteins. Various microtubule associated proteins (MAPs) bind to particular parts of the tubulin monomer and can greatly influence both microtubule dynamics and motor motility. The tau protein is one such MAP, which is particularly important in microtubule stabilization. Defective tau proteins can lead to diseases such as Alzheimer's*(4)*. Tau has also been shown to interfere with the motility of both kinesin and dynein, although kinesin is much more affected by tau interactions*(5, 6)*. Tau has six different isoforms, depending on how the exons are spliced during DNA transcription. The longest isoform is known as 4RL, while the shortest is known as 3RS. The 3RS tau isoform has been shown to affect kinesin motility much more drastically than the 4RL isoform*(5)*. Varying the tau concentration or type of isoform bound to microtubules could be one important way that motor transport of kinesin and dynein is regulated in the cell.

Section 1.3 Kinesin

Kinesin is a relatively simple and well-understood motor protein. Discovered in 1985, kinesin is a ~360,000 Dalton heterotetramer made up of two identical heavy chains of ~960 amino acids, and two identical light chains (see Figure 4). The heavy chains are the most important for motor function, and include the motor domain "head" made up of ~340 amino acids, which also is the site of ATP hydrolysis. The two light chains are involved with regulation and the binding of kinesin to cargo.

Each kinesin heavy chain is composed of an amino-terminal globular head region which binds to microtubules and hydrolizes ATP as kinesin takes a step, followed by a long alpha helical region which enables dimerization with the other identical heavy chain through the formation of a coiled-coil structure. The coiled-coil region is followed by a carboxy-terminal tail domain, which is the area that binds to cargo.

The coiled-coil region of the heavy chain is interrupted by two flexible hinge regions. When not bound to a cargo, kinesin becomes inactive by folding over at these two hinge regions, preventing ATP hydrolysis as the tail domain comes into contact with the motor domains.

A functionally processive kinesin construct can be created by truncating the heavy chain, leaving only about the first 400 amino acids*(7)*. This region includes the "head" and only a short coiled-coil region, but can walk and generate force similar to full-length kinesin. The other parts of the kinesin heavy chain and the light chain are important for regulation and cargo binding but are not essential for motility.

Kinesin walks along a microtubule as the microtubule binding domains (or "head" regions) bind and unbind from alpha-tubulin subunits along the track. Kinesin walks in hand-over-hand motion*(8)*, meaning that the leading head and trailing head pass each other with each step. Kinesin is known to take 8 nm steps*(9)* and to hydrolyze a single ATP molecule per step*(10-12)*. The state of the ATP nucleotide bound to the head determines the head's affinity for binding to the microtubule.

Kinesin is extremely processive; a single kinesin motor can take ~100 steps before dissociating from the microtubule. To achieve this processivity, the two heads must coordinate their stepping to prevent both releasing the microtubule simultaneously (and thereby causing the kinesin to fall off the microtubule). There is evidence to suggest that the two heads are "gated" by intramolecular strain*(13-16)*. When the trailing head releases from the microtubule, it creates a strain on the leading head that prevents it from binding ATP, thus ensuring that it remains firmly bound to the microtubule until the other head is also safely attached.

A model for the stepping cycle of kinesin goes as follows*(17)*: ATP binding to the leading head causes a conformational change in the neck linker region (the region bridging the head and tail regions of the heavy chain) that generates a "power stroke," followed by a biased diffusional search of the trailing, ADP-bound head to the next binding site on the microtubule. ADP is then released, and the new front head binds tightly to the microtubule. This causes internal strain which prevents ATP from binding to the front head until the rear head has hydrolyzed its ATP and the phosphate is released, leaving the rear head bound with ADP. The affinity for microtubules is weak in the ADP bound state, so the rear head dissociates, relieving strain and allowing the leading head to bind ATP. This starts the cycle over again, with the two heads having exchanged positions, and allowing the kinesin to walk in a hand-over-hand fashion.

The kinesin motor almost always steps towards the + end of the microtubule. As it does so, kinesin walks along a single protofilament within the microtubule*(18)*. A very processive and robust motor, a single kinesin has an average run length of approximately 1 μm and moves at an average velocity of about 600-800 nm/sec*(19)*. It can pull with a force of up to 5-7 pN*(20, 21)*, after which the motor stalls and ceases to take forward steps. Kinesin has been shown to take occasional back steps under high forces*(21, 22)(21)*

{{59 Meyhofer,E. 1995}}, although this is rare—in general kinesin is an extremely processive plus-directed motor.

The kinesin superfamily of proteins actually encompasses several different specific motor proteins, each involved with a different motility-based task within the cell. Fifteen different families of kinesin have been discovered. Kinesin-1 is known as conventional kinesin, and is the motor involved with transporting melanophores, lipid droplets, endosomes, and other cargos from the cell nucleus out to the periphery of the cell. Other types of kinesin are involved in tasks such as chromosome separation, microtubule depolymerization, retrograde organelle transport, axonal elongation, and many others, but will not be discussed in depth in this paper. For the purposes of this paper all references to "kinesin" will refer to Kinesin-1.

Section 1.4 Dynein

Dynein, in contrast to kinesin, is a much more complicated and poorly understood motor protein. While kinesin shares an evolutionary history with myosin (another simple motor

protein that walks not on microtubules but on actin filaments*(23)*), dynein is actually of the AAA+ (**A**TPases **a**ssociated with diverse cellular **a**ctivities) ATPase family*(24)* and is structurally very different from kinesin (see Figure 5). In fact, dynein is comparatively monstrous in size—roughly 1.2M Daltons in molecular weight and consisting of two heavy chains of about 520 kDa in mass (which are responsible for ATP hydrolysis and motor activity), as well as two ~74 kDa intermediate chains, four ~55 kDa light intermediate chains, and several light chains per motor. The function of the light and intermediate chains is not well understood but is thought to aid in cargo binding and regulation of the motor domains. In addition, a second protein known as dynactin is known to associate closely with dynein in cells. Dynactin is necessary for retrograde transport of cargos in live cells*(25, 26)*, has been shown to increase the processivity of dynein*(27, 28)*, and contributes to regulation*(29)* and cargo recruitment*(30)*.

Dynein does share some similarities with kinesin, in that it is formed by two main heavy chains which dimerize together, each with a "head" region that interacts with the microtubule on one end and a dimerized "tail" region which binds to various cargos on the other. Like kinesin, dynein walks in a hand-over-hand fashion along microtubules*(31)*.

Unlike kinesin, however, the microtubule binding domains on the dynein heavy chains are separated from the ATPase region by a 10-15 nm long stalk, and it is not known how the force is transduced through this distance to generate movement. The motor domain of dynein is ~10 times larger than that of kinesin, due to the presence of several ATP

binding sites. Like in other AAA+ proteins, the ATPase region of dynein forms a ring*(32, 33)*, with six possible ATP binding sites, known as sites 1-6. Site 1 has been shown to be the main ATP hydrolysis site and essential for dynein motility, although sites 2-4 can also bind nucleotides and seem to influence motility and be important in regulation of the motor*(34-36)*. In particular, ATP binding at site 3 is necessary for motility *in vivo(37)*. Sites 5 and 6 have degenerate ATP binding regions and are less likely to bind ATP but may perform structural roles.

Despite the fact that dynein was discovered nearly 20 years before kinesin, many questions remain regarding the details of dynein's function. Dynein (so named because of the force that it generates, *i.e.* "dyne"-force, "-in"- protein)*(38)*, was first discovered in axonemes in 1963*(39)*, where it functions not as processive motors but as groups of dimers and trimers which generate force to create axoneme movement in flagella, for instance. Twenty-four years later, in 1987, a different type of dynein known as cytoplasmic dynein was discovered to be a processive molecular motor, moving cargos along microtubules in the retrograde (towards the cell nucleus) direction*(40)*. Although many single molecule dynein fluorescence and optical trap studies have been done, they disagree on several important points.

For instance, studies disagree as to the step size of dynein. Some studies have found that dynein walks in 8nm steps*(31)*, while others show a broad distribution of step sizes that could even depend on the force which is exerted on the molecule*(41)*. The stall force of

dynein is still contested as well; although the consensus generally seems to be ~1-2 pN*(41)*, other groups have measured a stall force of ~7 pN for mammalian dynein*(31)*.

Part of the confusion could arise due to differences between the studies in species from which the dynein was purified. Indeed, yeast dynein and mammalian dynein certainly behave quite differently in terms of step size (clear 8 nm steps versus a wider distribution), velocity (~100 nm/s versus ~800 nm/s), and stall force (5-7 pN versus 1-2 pN). The discrepancies mentioned above apply to studies all done on mammalian dynein, but it is possible that different species (porcine versus bovine, for instance) even within the mammal kingdom differ in these key areas.

Several studies have shown that dynein is capable of taking backwards steps, either when under backward load (yeast)*(42)* or even under no load at all (mammalian)*(43, 44)*. In mammalian dynein, this backward motion often occurs in long segments of up to >1 micron in length*(43, 44)*. This bidirectional motion of dynein may be processive at least some of the time and has been shown to be ATP dependent*(44, 45)*, although much of the observed backwards motion could be due to 1-D diffusion along the microtubule*(43, 46)*.

Dynein is a much bigger molecule than kinesin and has a much higher degree of flexibility. Beads carried by dynein have shown a high level (~100 nm) of "flop", particularly in the direction perpendicular to the microtubule direction*(43)*. Importantly, dynein (both yeast and mammalian) has been shown to take off-axis steps from one

protofilament to another as it traverses a microtubule track*(45, 47, 48)*. This is in contrast to kinesin, which always walks along a single protofilament*(18)*.

Again unlike kinesin, cytoplasmic dynein exists as only one main type in the cell (as opposed to a whole superfamily of kinesin types). The greater flexibility and complexity of dynein may be due to the fact that it is called upon to perform many different types of tasks inside the cell. In addition to the transport of cargos from the outside of the cell towards the nucleus, dynein is also crucially important in chromosome segregation, mitotic spindle orientation, nuclear migration, and cellular migration*(49)*. There are different types of kinesin which perform each comparable role, but the same dynein molecule is able to complete a wide variety of jobs inside the cell, which may be why such a complex and large molecule is required.

Section 1.5 Saltatory motion

One might assume, given the knowledge of kinesin and dynein as plus and minus directed motors, that all that is required for efficient transport of cargoes inside the cell is to attach either kinesin or dynein to a cargo, depending on its intended destination (see Figure 6). Cargos headed towards the nucleus get picked up by a dynein, and cargos destined for the cell periphery are attached to a kinesin, and everything moves simply along.

In reality, however, the scenario is actually quite a bit more complicated. Cargos in general do not have *either* kinesin or dynein attached to them; rather, *both* kinesin *and*

dynein are generally found attached to the same cargo. Additionally, vesicles and other cargos in the cell exhibit a complex type of motion that is not simply inwards or outwards over large distances. Instead, the cargos are seen to move back and forth along a microtubule in a jerky stop-and-start fashion, with repeated direction reversals interspersed throughout. This bidirectional, jerky movement is known as saltatory motion and is common in eukaryotic cells*(50)*.

There are various ideas to explain why this type of motion might take place instead of the simpler smooth travel one might expect. One such theory is that this type of motion essentially creates an active diffusion*(51)* within the cell, allowing cargos to spread evenly throughout the cell, sampling a great number of locations much more rapidly than passive diffusion would allow in such a viscous and crowded environment. Another idea is that these pauses and reversals are caused by roadblocks within the cell, and that the saltatory nature of the cargo movement is a mechanism whereby the motors can bypass these obstacles*(52)*. Also possible is that saltatory motion acts as an "error-checking" method*(52)* whereby a cargo that is transported to the wrong destination can "rewind" and try again to reach the correct one. If bidirectional motion was not possible, such a mis-delivered cargo would be stuck at the first destination rather than being able to sample a larger range of possible end-points until it finally finds the correct one.

Whatever the answer is to *why* saltatory motion occurs in cells, an equally important and as-yet unanswered question is *how* this motion occurs. There are two main theories as to

what governs the bidirectional motion of cellular cargos: the coordinated motion model and the tug-of-war model.

1.5.1 Coordination Model

The coordination model assumes that it would be too inefficient for the motors to be simultaneously pulling in opposite directions, and that there is likely some sort of mechanism in the cell to turn one set of motors on and one set of motors off at any given instant (see Figure 7A). This mechanism could be some sort of accessory protein also attached to the cargo, which activates and inactivates in turn the kinesin and dynein such that they are never pulling simultaneously. Outside signals could trigger these additional proteins to activate or inactivate a particular motor, thereby giving the cell an efficient way of controlling the cargo behavior and of getting it to where it needs to go.

1.5.2 Tug-of-War Model

In contrast, the tug-of-war model (see Figure 7B) argues that the motors do not have any extra mediating proteins controlling whether they are active or inactive. Instead, this model assumes that the motors undergo a constant pulling match, and whichever motor (or group of motors) exerts the most force "wins", leading to the cargo moving in that direction for a time. In this model, direction reversals are caused by motors dissociating or binding from the microtubule stochastically, which tips the balance of force and leads to one side overpowering the other. No extra mediating factors are involved in switching the motors on or off, which means that extra energy is expended as motors work against each other.

1.5.3 Evidence for Coordinated Motion

A study done on squid axon vesicles in 1996 *(53)* showed that only plus-end directed movement occurred when both kinesin and dynein were present on either beads incubated with squid axoplasm or vesicles isolated from axons. The authors concluded that dynein was unable to compete with kinesin in a tug-of-war.

In 2002 Steven Gross' lab found that when they mutated dynein and dynactin in a cell to impair minus-end directed movement of liquid droplets in *Drosophila* cells, the result was not an improvement in plus-end directed motion of the liquid droplets as one might expect, but instead a severe impairment of plus-end directed motion. They concluded that a mutation that decreased the stall force of dynein should make it easier for kinesin to win a tug-of-war, and thus that their results were not consistent with a tug-of-war model*(54)*. Several similar studies have shown inhibition or depletion of kinesin abolishes dynein driven cargo transport and vice versa *(55-58)*.

In 2005 our lab published a paper *(59)* which applied FIONA to labeled peroxisomes inside live *Drosophila* S2 cells and measured the step sizes of the peroxisomes as they made bidirectional processive runs. Step sizes were found to remain constant at ~8 nm in either direction. Because compliance in the motor stalks could cause a degradation of step sizes if motors were acting simultaneously and in opposite directions, the constancy of the step sizes was inferred to indicate that no tug-of-war was taking place.

Levi et al. found in 2006*(60)* that melanosomes moving inside *Xenopus* cells exhibited velocity distributions with peaks corresponding to the number of active motors on the melanosome. They found that the number of active dynein motors increased when melanosomes traveled in the negative-end direction, while the number of active kinesin-2 motors remained the same no matter the direction of travel. They concluded that some mechanism was regulating the number of active dynein motors in order to coordinate the direction of movement. Because the kinesin-2 velocity profiles did not change when the number of dynein motors increased, they asserted that the two motor types did not compete but were carefully regulated.

A study done in 2009*(61)* found that microspheres positioned on the plasma membrane of immobilized paralyzed *Chlamydomonas* flagella did not exhibit direction reversals, and quiescent periods separated every transport event. The authors interpreted this to mean that the microspheres were transported by coordinated and exclusive motion of only a single motor type at a time.

1.5.4 Evidence for Tug of War

For some years the tug-of-war model was not favored because it was assumed that this model would imply that the motors would spend much of the time stuck at an impasse between balanced forces, with much energy wasted in the process. In addition, the complexity of the saltatory motion seen in live cells in response to various stimuli or to mutations in either motor type seemed impossible to explain via a simple tug-of-war model.

However, in 2008 Lipowsky *et al.(62)*published a paper in which they modeled a simple tug-of-war system with the assumption that the motors interact only mechanically via their attachment to the same cargo. They found that rather than creating frequent, long-lived stuck states, this model predicted a high probability of having only one motor type engaged at a time, in agreement with *in vivo* motility data. This result was due to a dynamic instability arising from the strongly nonlinear force-dependence of the single-motor unbinding rate. In other words, as soon as the forces become unbalanced (by the stochastic binding and unbinding of motors from the microtubule), the "losing" side motors are quickly ripped off the microtubule to give the opposing motors free reign to walk for a time. Eventually, some or all of them will stochastically unbind and opposing motors will bind. When the balance of forces is tipped, the new winners rip off the losers and so forth. They found five stable states: fast plus-directed motion, plus with pauses, no movement (stalled), minus with pauses, and fast minus-directed motion.

This paper showed that, in fact, a simple tug-of-war model could replicate many of the complex characteristics of *in vivo* saltatory motion; small changes in parameters such as stall force or microtubule affinity of each motor type led to qualitatively different types of bidirectional motility. Thus, the cell could easily regulate the directionality of motion simply by regulating the number of each type of motor attached to a cargo, or by altering the motile characteristics of the motors (for instance, affecting some change that slightly decreased the stall force of one type of motor).

Experimental evidence for a tug-of-war is also available. An early study done by the Vale lab*(63)* showed that when both dynein and kinesin motors were attached to a glass coverslip, microtubule movement continually switched direction, with long (micron-scaled) unidirectional run-lengths between direction reversals. The balance of forces did *not* produce little or no net movement, and the number of motors as well as their microtubule attachment times were the determining factors in which direction predominated.

Interestingly, Ally *et al*.*(64)* found, like earlier studies (see above), that impairment of one motor type also inhibited motility in the other direction. However, they also found that replacing one motor with a completely different motor type of the same polarity rescued the cell's ability to produce bidirectional movement. Cargos in which one type of motor was replaced by non-functional motors of the same polarity did not display bidirectional motion, however. This showed that plus and minus directed motors must be mechanically activated by the presence of a functional motor of the opposite polarity on the same cargo. It also showed that the inhibition of motion in both directions due to the impairment of one type of motor as discussed above does *not* require that a mediating protein regulates the pair of motor types. Such a mediating protein would not likely be able to regulate the unrelated replacement motors.

Another important study*(65)* provides evidence in favor of the Lipowsky tug-of-war model. Here, the authors took measurements of endosomes inside live cells, in a cell extract, and with purified motors, and found a distinct triphasic behavior (fast movement

in one direction followed by a slow segment and then fast movement in the opposite direction). The slow segments showed visible endosome elongation in the direction of motion, showing that the two motors clearly apply opposite forces during this period.

Another recent study*(66)* analyzed the motion of purified neuronal transport vesicles. They found that the vesicles generally had 1-4 motors of each type bound, and that the purified vesicles behaved *in vitro* very similarly to what is seen *in vivo*. The vesicles moved with robust bidirectional motion without any regulating factors present in the cytoplasm (although a regulatory complex could have been present on the vesicles themselves), with a small complement of motors. They found that their data was consistent with the Lipowsky model and with Soppina *et al*.

Two studies published this year also have results consistent with the tug-of-war model. In Schuster *et al*., bidirectional early endosome transport in fungal *Ustilago maydis* cells was found to be controlled by transient binding of dynein*(67)*. Their data was consistent with a stochastic tug-of-war, the outcome of which was governed only by the number of dynein bound to the cargo. Falleson *et al*. also supports the Lipowsky model*(68)*. This paper studied the force-velocity relationship of multiple kinesins transporting a microtubule in a gliding assay. The authors found that the velocity distribution changed under load and that under low load, the average number of bound kinesin underwent rapid fluctuations, consistent with the predictions of the Lipowsky model.

Section 1.6 Introduction to Experimental Techniques

1.6.1 Total Internal Reflection Microscopy*

Total Internal Reflection (TIR) microscopy is a crucial technique in the field of single molecule biophysics. It allows the imaging of molecules that are attached to a surface while excluding fluorescence in the solution above the surface. With traditional epifluorescence microscopy, a laser beam is used to excite fluorophores in a sample; however, many fluorophores in solution above or below the focus plane are also excited, leading to high levels of background fluorescence and therefore a poor signal-to-noise ratio. Total Internal Reflection (TIR) microscopy solves this problem by sending the laser beam in to the glass-water interface at such a steep angle that TIR is achieved. With TIR, only a thin layer of light (of exponentially decreasing magnitude) called the evanescent wave penetrates into the sample. This evanescent wave excites fluorophores close to the surface of the slide, but will not excite any fluorophores more than about 100 nm away from the surface. In this way, excellent signal to noise ratios and high levels of photon are achieved (see Figure 8).

1.6.2 FIONA

In order to conduct single molecule studies, researchers are confronted with the diffraction limit of light. For visible optical microscopy, this limit is $\lambda/(2*N.A)$, where λ (the wavelength of the light) is approximately 500 nm and $N.A$ (the numerical aperture of the microscope objective) is about 1.4. Diffraction limited spots in a traditional light microscope are therefore generally larger than 200 nm in diameter—

* Note: Sections 1.6.1 and 1.6.2, including Figures 8, 9, and 13 are reproduced (with some changes) with permission from a book chapter (in press) written by the author: "Fluorescence Imaging with One Nanometer Accuracy: In Vitro & In Vivo", *Single Molecule Enzymology*: Methods and Protocols, Springer Publishing Group.

much bigger than the molecules of interest. This resolution limit means that two identical fluorophores in close proximity can therefore not be distinguished using traditional light microscopy unless they are greater than ~250 nm apart. **F**luorescence **I**maging with **O**ne **N**anometer **A**ccuracy (FIONA) is a simple but versatile technique for achieving nanometer precision at biologically-relevant timescales. FIONA does not improve the resolution of fluorophores in close proximity but instead improves the localization accuracy of a single fluorophore.

FIONA enables the localization of a single molecule to within 1.5 nanometers and with 1-500 msec temporal resolution*(69)*. Data can be taken inside or outside of live cells at a timescale that is physiologically relevant, making FIONA an extremely valuable tool in the toolbox of single molecule research techniques. The principle behind FIONA is simple. In a typical FIONA measurement, a fluorophore is attached to some biological molecule of interest. As the biological molecule (and the attached fluorophore) moves through space, the center of its emission is continuously localized, making it possible to track single biomolecules with great precision. At the core of the technique is the ability to collect a large number of photons emitted by a single fluorophore. When we plot the number of photons emitted by a fluorophore versus its position in the x-y plane (Figure 9), we can localize the center of the resulting Airy function much more accurately than the width of the function. (A 2-D Gaussian function is often used to approximate the Airy function, with little error.) Theoretically, the accuracy with which it is possible to locate the center is the standard error of the mean, *i.e.*, the standard deviation divided by the square-root of the total number of counts. Thus, the accuracy of FIONA depends on

the collection of large numbers of photons. For 10,000 photons collected, for example, one obtains an accuracy of approximately 250/100 = 2.5 nm.

To be slightly more quantitative, in practice the accuracy depends on three factors, as shown in the equation below: the number of photons (N); the effective pixel size of the detector, *a*, which is the pixel size divided by magnification; and the standard deviation of the background, *b*:

$$\sigma = \sqrt{\left(\frac{s_i^2}{N} + \frac{a^2/12}{N} + \frac{8\pi s_i^4 b^2}{a^2 N^2} \right)}$$

σ is the uncertainty or standard error of the mean, *a* is the effective pixel size of the detector (pixel size divided by magnification), *b* includes both the background fluorescence and the detector noise, and s_i is the width of the distribution (which is approximately 250 nm for a diffraction limited spot of visible light) in direction *i*, where *i*=x or y. The first term ($\frac{s_i^2}{N}$) is due to photon noise, the second term is the effect of a finite pixel size of the detector, and the third term is the effect of background. Assuming an appropriate effective pixel size (of 80-120 nm, or 16 μm divided by the magnification, *e.g.* 160X) is used, the second term does not contribute significantly. When appropriate techniques are used to minimize background noise (as discussed below), the first term (photon noise) is the limiting factor in a FIONA measurement.

Thus, it is crucial to both decrease the background and collect as many photons as possible from the single fluorophores in order to obtain the greatest accuracy of localization possible. Several considerations must be made: first, an appropriate

fluorophore must be chosen—for accurate FIONA measurements to be made, the fluorophore must be sufficiently bright and highly photo-stable. Oxygen scavenging systems and other chemicals are generally needed to increase the lifetime and stability.

Second, background fluorescence must be minimized. This is typically achieved by the use of a Total Internal Reflection (TIR) microscope, which (as discussed above) allows the imaging of molecules that are attached to a surface while excluding fluorescence in the solution above the surface. Hence, the excellent signal to noise ratio and high levels of photon collection required for the FIONA technique are achieved (see Figure 8). Careful cleaning of sample chambers and efficient surface blocking to avoid non-specific binding of fluorescent molecules must also be employed to minimize background fluorescence, since impurities on the surface are within the evanescent wave and can decrease the signal- to-noise ratio, even when using TIR microscopy.

Third, sensitive photon detection is required, usually in the form of an electron multiplied charge-coupled device (EMCCD) camera. Back-thinning of EMCCD cameras allows a quantum efficiency of ~90%. In addition, electronic cooling to ~-70° C virtually eliminates dark current, while electron multiplying enables very sensitive detection of photons.

Once a sufficient number of photons can be collected, a researcher can use FIONA data analysis techniques to localize and track the particles in the images that have been recorded. A localization measurement with a standard error of 1-2 nm can be achieved

using a laser in the visible spectrum, an effective pixel size of 80-120 nm, a TIR microscope and an EMCCD camera to minimize background, and a sufficiently bright fluorophore to obtain ~10,000 photons per frame. These tools allow single molecule tracking of molecular motors or other proteins with excellent spatial and temporal accuracy.

Although a number of different enzymes can be studied using FIONA, molecular motors are particularly well suited to this technique. Using FIONA, they can be precisely tracked as they move in a cell or in an artificial cell-like environment. For instance, a kinesin molecule can be tracked as it walks on microtubules laid down on a prepared coverslip. The spatial and temporal precision gained by applying the FIONA technique reveals valuable information about the motors, such as the distance traveled with each step, the pause times between steps, or even details such as whether the monomers pass each other with each step*(8)*—information that cannot be determined using traditional microscopy-based measurements. The study of molecular motors can be greatly enriched by the precise localization measurements which FIONA makes possible.

1.6.3 Optical Trapping

Optical traps are very useful tools for studying single molecules, particularly molecular motors*(70)*. Optical traps function by drawing in and trapping a small translucent particle into a tightly focused, infrared laser beam. The particle's position can be manipulated by translating the focus of the beam, and by measuring the refraction of the laser due to the

presence of the bead, one can extract both the displacement of the particle away from the center of the focus as well as the force exerted on it.

Optical traps work by taking advantage of the difference in index of refraction of a particle (such as a polystyrene sphere) and the surrounding media (usually water). The focus of the laser also provides a spatial photon gradient. Since the bead is composed of dielectric material, when the light from the laser beam passes through it, it induces electric dipoles. These induced electric dipoles will cause a force on the bead due to the electric field gradient, causing it to be continuously pulled back to the center of the laser beam focus, where the gradient is strongest.

This can be illustrated by a simple ray diagram (see Figure 10). The laser beam is diffracted by the bead due to the difference in index of refraction, meaning that it exits in a different path than it entered. The change in momentum of the light means that there must be an equal and opposite change of momentum on the bead. If we sum up the changes of momentum due to all the photons, we end up with a net force towards the center of the trap (the beam's focus.) For small displacements, the force exerted on the bead can be modeled as a simple spring, meaning there is a restoring force proportional to the displacement from the center of the trap. The effective spring constant is called the trap stiffness.

Since the refraction of the light due to the bead's presence changes the angle of the exiting laser beam, we can measure the displacement of the bead from the center of the

trap by measuring the deflection of the bead with a lens and a quadrant photodiode (QPD). Then, using the position of the bead thus measured and stiffness of the trap, we can also determine the force exerted on the bead. All this can be done in real time, with very fast acquisition rates (in this paper, 4000 Hz), allowing for very precise measurements of single particle motor behavior.

Chapter 2: Materials and Methods

Section 2.1 Protein Purification and Preparation

2.1.1 Full Length Kinesin

Full-length kinesin was purified by collaborators (Kathy Trybus lab, University of Vermont) as described*(71)*. In brief, the mouse brain kinesin KIF5B heavy chain (Invitrogen, accession number BC090841) with a C-terminal hexa-HIS tag and kinesin light chain 2 gene (ATCC, accession number BC014845) were cloned into separate baculovirus transfer vectors (pAcSG2, BD Biosciences). Sf9 cells were co-infected with recombinant baculovirus coding for HIS-tagged kinesin heavy chain and YFP-tagged light chain, and grown in suspension for 72 h. Cells were sonicated to lyse, and the cell lysate was centrifuged at 200,000 rcf for 30 min. The supernatant was applied to a HIS-Select® nickel affinity column (Sigma–Aldrich). The resin was washed with buffer containing 30 mM imidazole. Kinesin was eluted from the column with 10 mM sodium phosphate, 200 mM imidazole, pH 7.5, 0.3 M NaCl and 1 μg/mL leupeptin. The fractions of interest were combined and concentrated, then dialyzed in 10 mM HEPES, pH 7.3, 200 mM NaCl, 50% glycerol, 1 mMDTT, 10 μM MgATP and 1 μg/mL leupeptin for storage at −20°C.

2.1.2 Truncated Kinesin Constructs—K432 or K560

Truncated kinesin was purified in our lab by Marco Tijoe. Truncated kinesin constructs were purified according to the procedure outlined by Pierce and Vale*(72)*. The gene for

the kinesin heavy chain was truncated at either at amino acid 432 or 560, with a His tag followed by a biotin tag at the C terminus (K432), or with a GFP and 6x His at the C terminus (K560), and inserted into pET21a plasmid and then transformed into BL21 cells and plated onto antibiotic selection plates. Single colonies were grown in LB media to OD 0.4-0.8, at which point protein production was induced by addition of IPTG. 3-5 hours after induction, cultures were pelleted by centrifugation, resuspended in lysis buffer (50 mM NaH2PO4, 300 mM NaCl , 10 mM imidazole, 40 μM MgATP, 1 mg/mL lysozyme, 1 mM PMSF, 0.1 mL Protease Inhibitor Cocktail (Sigma Aldrich, P8849), pH 8.0), and sonicated using a probe tip sonicator. The lysate was pelleted and the supernatant was mixed with a Ni-NTA slurry for one hour. The slurry was poured into a column and washed three times with low imidazole concentration (20mM). The protein was then eluted from the column with a high imidizole concentration (250mM). Protein purification was checked with SDS-PAGE and concentration was measured using the Bradford Assay.

2.1.3 Mammalian Dynein

Bovine brain dynein was purified by collaborators (Trina Schroer lab, Johns Hopkins University) as described*(73)*. Briefly, bovine brains were homogenized and centrifuged to clarify. The supernatant was loaded onto a SP-Sephadex Fast Flow chromatography column. The 0.5 M KCl fraction was layered over sucrose gradients and centrifuged. The column/sucrose gradient step was repeated. Sucrose gradients were then fractionated, with each fraction run on a SDS-PAGE gel. Fractions containing predominantly dynein were pooled, loaded onto a Mono-Q ion exchange column, and the

peaks separated. The sucrose gradient fractionation and ion-exchange chromatography was repeated until the dynein was free from any dynactin or kinesin contamination, as seen on an SDS-PAGE gel*(41)*.

2.1.4 Yeast Dynein

Yeast dynein was purified by collaborators (Ahmet Yildiz lab, UC-Berkley) as described*(47)*. To construct the truncated dynein (Dyn1331kD), the 5' end of the DYN1 hapolid yeast cell dynein gene was deleted by homologous recombination, leaving base pairs 3655-12779. To artificially dimerize Dyn1331kD, a sequence encoding GST was added just upstream of the dynein sequence. A HaloTag was also added. To allow for purification, a ZZ tag (two copies of the IgG binding domain of protein A), a TEV protease cleavage site with a short linker, GFP, and a 2xHA tag were added to the 5' end of the constructs. Truncated dynein was expressed behind the galactose promoter.

To purify the protein, yeast cells were grown to an OD600 between 1.2 and 2.0, then harvested by centrifugation, washed once with water, resuspended in 0.2 volumes of 5X dynein lysis buffer (1X dynein lysis buffer: 30 mM HEPES (pH 7.2), 50 mM KAcetate, 2 mM MgAcetate, 1 mM EGTA, 10% glycerol, 1 mM DTT, 0.5 mM Mg-ATP, 1 mM Pefabloc, 10 μg/ml Leupeptin, 10 μg/ml Pepstatin A), and frozen by drops in liquid nitrogen. The pellets were lysed by grinding with a mortar and pestle, then centrifuged at 290,000 x g for 15 min. The supernatant was then incubated with IgG sepharose (Amersham Pharmacia) for 1 hr at 4°C. The IgG beads were washed four times with dynein lysis buffer supplemented with 250 mM KCl, washed twice with TEV cleavage

buffer (10 mM Tris (pH 8.0), 150 mM KCl, 0.5 mM ATP, 1 mM DTT, 1 mM Pefabloc), and incubated with TEV protease for 1 hr at 16°C. The resulting supernatant was then incubated with bovine microtubules (330 μg/ml) in the presence of apyrase (6.6 U/ml) and 20 μM paciltaxel at room temperature for 10 min. This mixture was then centrifuged over a 40% sucrose cushion at 104,000 x g for 15 min. The resulting pellet was resuspended in dynein lysis buffer supplemented with 100 mM KCl, 5 mM MgATP and 20 μM taxol. After incubation at room temperature for 10 min, the mixture was centrifuged at 104,000 x g for 15 min and the resulting supernatant was aliquoted and frozen in liquid nitrogen. Approximate yield was ~25 μg/ 1 liter culture.

2.1.5 Tau Protein

Tau protein (4RL-tau isoform) was purified by collaborators in Chris Berger's lab (University of Vermont, Burlington, Vermont) as described*(74)*. Briefly, tau isoforms were expressed in BL21-CodonPlus(DE3)-RP E. coli cells (Stratagene, La Jolla, CA) using pET vector system (Novagen, Madison, WI). Cells were lysed, extracted proteins were boiled, clarified by centrifugation, passed through a 0.22 μm filter, and isolated by consecutive Q Sepherose®and SP Sepherose® Fast Flow columns (Sigma, St Louis, MO). Purified tau was dialyzed in BRB80 buffer, and purity was assessed by SDS-PAGE. Protein concentration was determined using the bicinchonic acid protein assay (Pierce, Rockford, IL).

Tau protein was labeled in our lab by incubating with 10X excess DTT for 2 hours at room temperature, followed by DTT removal by putting the sample through a Zebra

desalting column (Pierce, #89889), and incubation with 10X excess AlexaFluor 488 maleimide (Invitrogen, A10254). The sample was then passed through a Zebra desalting column a second time to remove excess dye, aliquoted into 5 µl aliquots, flash-frozen in liquid nitrogen, and stored at -80° C until just prior to use.

2.1.6 Axonemes

Axonemes were purified from sea urchin sperm as described*(72)*. Briefly, live sea urchins (*Strongylocentrotus purpuratus*, Pt. Loma Marine Invertebrates) were injected with 0.5M KCl. Semen was collected and pelleted by centrifugation, then repeatedly dounced in buffer 1(5 mM imidazole : CI-, pH 7.0, 100 mM NaC1, 4 mM MgSO4, 1 mM CaC12, 0.1 mM EDTA, 0.1 mM ATP, 7 mM 2ME) with 1% Triton X-100 and repelleted. The pellets were then resuspended and dounced in buffer 2 (5 mM imidazole: Cl-, pH 7.0, 600 mM NaCI, 4 mM MgSO4, 1 mM CaCI2, 0.1 mM EDTA, 7 mM 2ME, 1 mM DTT) pH 8.0 with 1% Triton X-100, then again in buffer 1 repeatedly. Finally, axonemes were resuspended in buffer 1 and mixed with 50% glycerol and stored at -80°C (long term) or -20°C (short term).

2.1.7 Microtubules

Microtubules were prepared from commercially purchased tubulin monomers (Cytoskeleton, TL238) by combining unlabeled tubulin with biotinylated tubulin (Cytoskeleton, T33P) and tubulin labeled with a hiLyte 488 fluorescent tag (Cytoskeleton, TL488M) in a 20:1:1 ratio with 50% glycerol, 1mM GTP (Cytoskeleton, BST06), and 1mM DTT. The solution was then incubated at 37°C for 30 minutes to

allow the tubulin to polymerize. Paclitaxel (Cytoskeleton, TXD01) was then added at a final concentration of 20 µM to stabilize the polymerized microtubules (paclitaxel is a potent inhibitor of tubulin depolymerization). The solution was centrifuged at 15,000 rcf for 30 minutes to pellet the microtubules. The supernatant was discarded, and the microtubules were resuspended in a 20 µm paclitaxel solution and stored in the dark at room temperature for 1-2 weeks.

Section 2.2 *In vitro* Fluorescence Experiments

2.2.1 Reversals

Beads with dynein and kinesin were prepared as follows (see Figure 11): Red carbolyxlated polystyrene beads with 500 nm diameter (Invitrogen F-8812) were diluted 2:5 into a solution of 8mg/ml Bovine Serum Albumin (BSA, Sigma #A7906) in DMB (dynein motility buffer, 30mM HEPES pH 7.2, 50mM KAcetate, 2mM MgAcetate, 1mM EGTA) and sonicated briefly. Dynein and/or kinesin proteins were diluted to the appropriate concentration (see below). The dynein motors were kept at ~500 nM concentration and the kinesin was diluted in DMB with BSA (8mg/ml) plus 20mM DTT (DL-Dithiothreitol, Sigma #D9779), then mixed with the dynein proteins at a final concentration of 6.6 nM. Finally, 1 µL of bead solution prepared as described above was mixed with the protein mixture and allowed to incubate at 4°C for ~30 minutes.

A "reference kinesin" solution (see Figure 12) was prepared by mixing 1 µL of 200 µg/mL penta-His antibodies labeled with AlexaFluor 647 (Qiagen, #126244141) with 1 µL of ~4.4 µM K432 protein prepared as described above. The solution was allowed to

incubate on ice ~30 minutes. 13.5 µL of BSA (8mg/mL) in DMB buffer was then added to dilute the protein to a concentration of ~0.28 µM.

Flow chambers were prepared by applying two pieces of double sided tape to a glass slide, and a glass coverslip was then sandwiched on top, leaving a ~20mm X 4 mm X 0.2mm channel between them (see Figure 13). The resulting flow chamber has a volume of ~20µL. A 1 mg/mL solution of BSA-biotin (Sigma-Aldrich, A6043) was flowed through the chamber using capillary action and allowed to incubate for ~5 minutes. The BSA sticks to the glass non-specifically, leaving a layer of biotin available for subsequent binding in addition to coating the glass to prevent other proteins from binding. The chamber was then washed with BRB80 buffer (80mM PIPES, 1mM EGTA, 1mM MgCl2, pH 6.9), followed by a 0.5 mg/mL solution of neutravidin (Pierce, #31000), which was incubated for ~5 minutes. Each molecule of neutravidin has four biotin-binding sites which attach the BSA-biotin layer. The biotin-avidin linkage is extremely stable, with a dissociation constant*(75)* of ~10^-14 mol/L, making the bond nearly as stable as a covalent bond. Following the addition of neutravidin, the chamber was again washed with BRB80, and biotinylated microtubules diluted 1:50 (final tubulin concentration 200 nM) into BRB80 with 20µM paclitaxel were added to the flow chamber and allowed to bind for ~10 minutes. The microtubules were then washed with BRB80 plus 20µM paclitaxel before introducing the final imaging buffer (see Figure 14).

To prepare the final imaging buffer, the following reagents were combined: 95 µL BSA (8mg/ml) in DMB buffer, 2 mM MgATP (Adenosine 5′-triphosphate magnesium

salt, Sigma #A9187), 20 mM DTT, 20 µM paclitaxel, and an oxygen scavenging system made up of 2.5 mM PCA (3,4-Dihydroxybenzoic acid, Fluka #37580), and 50 nM PCD (Protocatechuate 3,4-Dioxygenase, Sigma #P8279). 2 µL bead solution prepared as described above as well as 1 µL of 0.28µM reference kinesin preparation (see above) were then added. This imaging buffer was briefly sonicated in a bath sonicator cooled with ice prior to introducing the solution to the flow chamber.

Data was then taken on an inverted Olympus Ixon 70 microscope with a 100X 1.45 numerical aperature objective (PlanApo 100X 1.45 NA ∞/0.17) plus an extra 1.5x magnification. The sample was excited using TIR fluorescence (see introduction) by the following lasers in turn: 488 nm argon-ion (Melles Griot, 60mW, 543-AP-01), 532 diode (World Star Tech, 30 mW, model #TECGL-30), or 633 HeNe laser (Coherent HeNe laser, 4mW, model #31-2041-000). Laser powers were adjusted by inserting neutral density filters to achieve the desired power at the objective. Just prior to entering the objective, laser powers were: 240 µW (488 nm), 21 µW (532 nm), and 360 µW (633 nm). A z488/532/633rpc (Chroma) triple bandpass dichroic mirror was used inside the microscope in combination with a z488/532/635m (Chroma) triple bandpass emission filter. For each field of view, an image was taken using the 488 nm laser to excite the hiLyte 488-labeled microtubules (or the alexa488 labeled tau protein attached to microtubules) in combination with a HQ525/50M (Chroma) bandpass slide-in filter (to eliminate emission from the 500 nm beads, which can also be excited at this wavelength). The 633 nm laswer was then used to excite the alexa 647-labeled anti-His antibody attached to the "K432" truncated kinesin, used as a reference to tell the directionality of

the microbutules. The K432 movie also allowed us to exclude any microtubules of opposite polarity that might be overlapping or too close to tell apart in the 488 nm fluorescence image, as we could see areas with K432 traveling in both directions and therefore exclude them. Finally, the 532 nm laser was used to excite the 500 nm beads with motors attached. Several movies were taken using the 532 nm laser per field of view as the behavior of the motors on the beads was observed.

Movies were recorded using an Andor iXon EM + (DV-897E-CS0) camera with the following settings: Acquisition Mode: kinetic, Triggering: internal, Readout Mode: image, Number Prescans: 0, Baseline Clamp: on, Vertical Pixel Speed: 3.3 µsec, Vertical Clock Voltage Amplitude:normal, Readout Rate: 10MHz at 14 bit, Pre-amplifier Gain: 5.2x, Ouput Amplifier: Electron Multiplying, Electron Multiplier Gain: either 300 (for 488 or 633 nm excitation) or 10 (for 532 nm excitation), Acquisition Time: 0.1 second (unless otherwise noted).

2.2.2 Yeast Dynein Bead Experiments

For experiments using yeast dynein, streptavidin coated red 500 nm beads were used in place of carboxylated beads, and the samples were prepared as follows: 20 µL of a stock of 0.1% w/v 0.5 µm diameter, streptavidin coated Nile red fluorescent polystyrene particles (SVFP-0556-5, Spherotech Inc., LakeForest, IL) were added to 19 µL of DMB buffer and sonicated for 1 min in an ice-cooled sonicator bath. 1 µL of a 1 mg/mL stock of biotinylated anti-histidine antibody (MCA1396B, AbD Serotech, Raleigh, NC) and 10 µL of a 0.1 mg/mL stock of biotinylated anti-GST antibody (MCA1352B, AbD Serotech,

Raleigh, NC) were then added and allowed to react for ~30 min at 4ºC. 50 µL of 8mg/mL bovine serum albumin (BSA) dissolved in DMB was added and incubated on ice for ~15 min and then centrifuged at 15,000 rcf for 15 min at 4ºC. The supernatant was discarded, and the pellet was suspended in 100 µL of 8 mg/mL BSA. The sample was again centrifuged at 15,000 rcf for 15 min at 4ºC and the supernatant discarded. The pellet was re-suspended in 9 µL of DMB buffer with 8 mg/mL BSA, 10 µM ATP, and 10 mM DTT. The beads were then sonicated for 1 min at ~4ºC. Yeast dynein and truncated kinesin were mixed, and 2.5 µL of this mixture was added to the beads and incubated on ice for ~3 hours. Beads were then again briefly sonicated before diluting into imaging buffer and flowing into the sample chamber (similar to the protocol above).

2.2.3 Tau Protein Experiments

Tau protein roadblock experiments were done as above except that microtubules were polymerized from unlabeled tubulin and biotinylated tubulin monomers only. Tau protein was diluted 1:1,000 to ~3.4 nM in BRB12 buffer (12mM PIPES, 1mM EGTA, 1mM MgCl2, pH 7.2) and mixed with 200 nM microtubules (final molar ratio of ~1:60) and allowed to incubate for ~30 minutes. The microtubule wash buffer and imaging buffer were each supplemented with tau protein as well (at the same concentration as was mixed with the microtubules).

Section 2.3 *In vivo* Experiments

In vivo experiments were performed in our lab by Ben Blehm. A549 cells (ATCC, CCL-185) were grown in F-12K medium supplemented with 10% Fetal Bovine Serum and antibiotics (Penicillin-Streptomycin at 100 IU/mL), at 37°C under a 5% CO_2 atmosphere. Cells were passaged weekly with .25% trypsin .53mM EDTA solution, and for experiments were grown on glass bottomed petri dishes (WilcoWells, HBSt-5040). The experiments were carried out at room temperature (22°C) on an inverted Nikon TE-2000U microscope, with a 1.2NA 60x water immersion objective, and imaged onto an Andor iXon CCD camera (DV887DCS-BV) with an acquisition rate of either 100 msec or 33 msec (only 50 second long, 100 msec/frame movies were analyzed for reversal statistics). Isolated lipid droplets were identified from the movies and excised for analysis.

Section 2.4 Optical Trap Experiments

Samples for use in the optical trap were prepared essentially as above, except that 1.2 μm diameter non-fluorescent carboxylated polystyrene beads (SVP-10-5, Spherotech Inc., LakeForest, IL) were used. For dynein-only piezo step-back experiments, protein was added at the same concentration as the fluorescence experiments (500 nM), and for kinesin-only piezo step-back experiments, the protein was diluted 10x more than for fluorescence experiments (0.66 nM). For mammalian dynein and kinesin experiments, ATP concentration was reduced to 20 μM final concentration, and 2mM creatine phosphate (Sodium creatine phosphate dibasic tetrahydrate, Sigma #27920) and 2U/ml creatine kinase (Roche #127566) were also included in the imaging buffer in order to create an ATP regeneration system. Reference k432 was omitted from the imaging

buffer, and beads were diluted an additional 20 times before adding to the imaging solution.

Since mammalian dynein often walks backwards as discussed above, to ensure we correctly determined the forward from backward stepping in the trap, we determined the directionality of each axoneme before beginning the experiment. For these mammalian dynein piezo-step back experiments, a reference kinesin sample was created by mixing full-length kinesin with smaller (500 nm) carboxylated beads and allowed to bind for 30 min on ice. These beads were then diluted 1:80 and 1 µL was added to the imaging buffer in addition to the larger dynein-only beads. These beads were easily distinguished from each other by the large difference in diameters, which could be seen in the camera using bright-field imaging. Before taking data for each dynein-only bead, a kinesin-only bead was brought down to the axoneme and allowed to bind. The directionality of the axoneme was determined by observing the direction of walking of the small bead. A large dynein-only bead was then brought to the same axoneme and used for the piezo-step back experiment.

For optical trap experiments with yeast dynein, 5 µL of a stock of 1% w/v 1.2 µm diameter, streptavidin coated polystyrene particles (SVP-10-5, Spherotech Inc., LakeForest, IL) were added to 25 µL of DMB buffer and sonicated for 1 min in an ice-cooled sonicator bath. 20 µL of a 0.1 mg/mL stock of biotinylated anti-GST antibody (MCA1352B, AbD Serotech, Raleigh, NC) was then added and the sample was allowed to react for ~15 min at on ice. 50 µL of 8mg/mL bovine serum albumin (BSA) dissolved

in DMB was added and incubated on ice for 10 min and then centrifuged at 15,000 rcf for 5 min at 4ºC. The supernatant was discarded, and the pellet was suspended in 100 µL of 8 mg/mL BSA. The sample was again centrifuged at 15,000 rcf for 5 min at 4ºC and the supernatant discarded. The pellet was re-suspended in 9 µL of DMB buffer with 8 mg/mL BSA, 10 µM ATP, and 10 mM DTT. The beads were then sonicated for 1 min at ~4ºC, and 1 µL of yeast dynein stock was added and incubated on ice for 2-3 hours. The beads were then again briefly sonicated. The remainder of the experiments were performed similarly to the mammalian dynein trap experiments described below except that the reference kinesin beads were omitted, saturating ATP concentrations were used (because of yeast dynein's slower stepping velocity), and the creatine phosphate and creatine kinase were omitted.

Flow chambers for optical trap experiments were prepared using axonemes as opposed to microtubules. To prepare the chamber, axonemes were diluted 1:30 in BRB80 buffer, flowed in the sample chamber, and incubated upside-down at 4°C for ~10 minutes. The surface was blocked with 8mg/mL BSA incubated for ~5 minutes. Imaging buffer was then flowed through the chamber just prior to data collection.

A custom built optical trap in our lab by Ben Blehm (who also collected all the optical trap data included in this study) and was used for force measurement and backward stepping experiments. The trap consists of a 1064 nm trapping laser (SpectraPhysics, Nd:YVO_4, PN# BL-106C) and an 845nm detection laser (Lumics, PN# LU0845M150-1G36F10A). The lasers were sent into a modified inverted Nikon TE-2000-U

microscope through a Nikon 60x 1.2NA water immersion objective. The trapping beam was positioned using a one-axis Acousto-Optic Modulator (Gooch & Housego, PN# 23080-3-1.06). A Quadrant Photo Diode in a plane conjugate to the back focal plane of the objective used for bead detection. Trap stiffness calibration was carried out by fitting a Lorentzian to the thermal noise of a bead in the trap (data acquisition rate of 80 kHz), while the Volts to nanometers calibration was carried out by oscillating the trap at 100Hz and comparing the known amplitude of oscillation to the bead's displacement as in [Tolic-Norrelke, Review of Scientific Instruments vol 77, 2006]. Backward stepping was simulated with a piezostage (Mad City Labs, stage PN# MCL 01069), controller PN# NanoDrive MCL 01312). Data acquisition, AOM control, and piezo control were carried out with a FPGA DAQ card and custom programs (National Instruments, PXI-7851R and Labview v8.5). Experiments were all carried out at room temperature (22°C) with a 4000Hz data acquisition rate. Trap stiffness was adjusted such that the motors could travel ~100 nm before reaching their respective stall forces.

Trap data was analyzed by first correcting for the compliance of the motors (1.06 for mammalian dynein*(41)*, 1.23 for kinesin*(9)*, yeast dynein uncorrected) and then binning by 10. The net motion of the motors were determined by subtracting the position of the piezo stage from the position of the bead at each time point. Steps were found by running a Student T-test fit program "MtltyAnalysis_ttest" written in IDL by Sheyum Syed in our lab in 2005. on the resulting traces. Parameters used to obtain the T-test fit were as follows:

```
mingrp=2 ;min and max numbers of data to be...
maxgrp=10 ;grouped together each time for analysis
```

```
minthrs=0.01; statistical threshold value...minimum
maxthrs=0.05; threshold maximum used in calcs
thrspoints=5; # threshold values @ which fits will be done
```

Traces were then scored as having a "snap-back" event if the T-test fit had at least one step with a size larger than a given threshold limit. Threshold limits were set at 50 nm, 75 nm, or 100 nm.

Section 2.5 Data Analysis

Fluorescence bead data was analyzed using a custom-written program created in Matlab. In brief, the program does the following (a more detailed explanation can be found in the Appendix):

2.5.1 Fluorescence Bead Program Summary

1. Finds the microtubules in an image, fits lines to them, and makes a "mask" to apply to other files so that only the spots on microtubules are analyzed. It records the position and angles of each microtubule.
2. Makes kymographs of labeled truncated kinesin moving on the microtubules as a reference to determine the + end of the microtubule and to exclude areas with two microtubules of opposite polarity that are close together or overlapping.
3. Finds moving spots on microtubules in the data files. It excises them and saves a copy of the movie.
4. Applies FIONA to moving spots and rotates the trace so that x is along the microtubule and y is perpendicular to it (with the + direction to the right), then plots x

position vs. time. Using the Recursive Douglas-Peucker Polyline Simplification algorithm (dsimplify.m by Wolfgang Schwanghart, http://www.mathworks.com/matlabcentral/fileexchange/21132-line-simplification), it finds segments of roughly constant velocity and generates histograms of various measures such as segment lengths, velocities, etc.

5. Locates places where the beads reversed direction by looking for places where the slope changes sign with some minimum distance traveled (*i.e.*, 250 nm or 500nm) on either side of the slope change.

2.5.2 *In vivo* Analysis

For *in vivo* experiments, lipid droplets were analyzed with FIONA. The x position vs y position plot was then fit to a straight line, and the axis rotated to horizontal. Lipid droplets were determined to be moving in the + or – direction based on if they moved mostly towards the cell periphery or interior, respectively. The x position vs. time trace was then plotted and analyzed according to the methods described above.

Chapter 3: Results

Section 3.1 *In Vitro* Saltatory Motion

3.1.1 Fluorescence Bead Assay Results

To assess whether additional regulating factors are required to mediate the up-and-back saltatory motion of cellular vesicles traveling on microtubules *in vivo*, we created a simplified *in vitro* system where kinesin and dynein are both attached to a single cargo—in this case, a 500 nm bead. Since no other accessory proteins are included in the system, we can assume that whatever behavior we see is due to the interaction between kinesin and dynein alone.

To this end, as described in Chapter 2:Materials and Methods, we attached both full-length mammalian kinesin and native bovine dynein via non-specific adsorption onto a carboxylated bead. We laid down fluorescent microtubules on a glass coverslip and assessed the polarity of the microtubules by observing the direction of motion of truncated kinesins attached to fluorescent anti-His antibodies. This reference kinesin also allowed us to exclude any areas where two microtubules of opposite polarity were overlapped or close together. We introduced the kinesin-dynein beads and observed their trajectories as they traveled along the microtubules via TIRF microscopy. We then applied FIONA to the point-spread functions of the beads and plotted the trajectories. We fit these trajectories to sections of roughly constant velocity and analyzed the results. (See Chapter 1: Introduction for information about these techniques and Chapter 2: Materials and Methods for a more detailed description of the experimental setup and analysis.)

Beads with both motors frequently exhibited bidirectional motion (See Figure 15). About one fifth (21%) of beads with both motors were observed to have at least one direction reversal (defined as two successive segments at least 500 nm in length with opposite directions) per trace (traces are fifty seconds in length, or as long as the bead remained in the field of view during the fifty second movie). This is in stark contrast to beads with kinesin only or dynein only, of which 0% (kinesin) and 5% (dynein) had one or more reversal (see Figure 16).

Since dynein motors are capable of walking backwards, it is important to assess whether the bidirectional motion seen could be due to dynein motors alone rather than to the interplay of both kinesin and dynein motors. To do this, we compared our results from beads with dynein only to those with both dynein and kinesin. We did observe that beads carried by dynein-alone can exhibit bidirectional motion, as previously described by other groups*(43, 44)*. However, beads with both kinesin and dynein exhibited more frequent bidirectional motion of longer length scales than did those with dynein alone (see Figure 17). In addition, the beads with both kinesin and dynein behaved significantly differently from those with dynein-only (or kinesin-only) in terms of net distance traveled (Figure 18). Even within the subset of traces exhibiting at least one reversal (see Figure 18, inset), beads with both dynein and kinesin had a significantly different net distance traveled than beads with dynein only. (This effectively excludes any beads in the kinesin-and-dynein sample that were more likely to have only kinesin or only dynein attached to that particular bead, thus excluding any effect due to simple averaging of the

results of dynein-only and kinesin-only beads. Instead, the dynein-and-kinesin sample clearly shows a distinct characteristic that can only come from the interplay of dynein and kinesin on a single bead).

The robust bidirectional motion we observed in our simplified tug-of-war system shows that such saltatory motion does not necessarily require any external signals or mediating proteins, as these were not present in our *in vitro* system.

3.1.2 Motor Concentration Determination

An important question to consider with our *in vitro* system is how many of each type of motor are involved with the tug-of-war we observe. This question is difficult to answer directly, however, because of the stochastic nature of the motor binding to the beads. However, the number of motors per bead is actually not the relevant quantity; rather, the number of motors which can simultaneously interact with the microtubule is the quantity that matters in terms of our tug-of-war assay. This number is certainly much smaller than the number of motors bound to the bead in total (since the bead is quite large, many motors that are bound to the bead are in fact quite far away from the microtubule). This number can also change over time. For instance, the bead might rotate slightly when one motor releases from the microtubule, allowing motors close by that were previously unable to bind to the microtubule to now have access.

We performed two measurements to give an indication of how many motors are simultaneously interacting with the microtubule. First, we performed a simple optical

trap experiment in which a number of beads are each held in turn over a microtubule and allowed to bind. We plotted the fraction of beads that do bind versus the relative concentration of the motor. The resulting graph (Figure 19) was fitted to a single Poissonian function, which shows that only a single motor is required for motility. The concentration used for the *in vitro* fluorescence assays is indicated in the figure. In other studies*(6, 43)*, a binding fraction of this amount corresponded to 1-3 motors simultaneously interacting with the microtubule per bead.

Second, we measured the stall forces of the motors attached to the beads. Since stall forces are additive, a histogram of the stall forces should have peaks of n*F where F is the stall force of a single motor and n varies from one to the maximum number of motors simultaneously pulling on the bead. Stall forces for beads with dynein only showed peaks at ~1.5 pN and ~3 pN, corresponding to 1 or 2 motors, respectively (see Figure 20). Beads with both dynein and kinesin (added in the same amount as above) showed mostly 1 motor stall forces in the minus direction, with some 2 motor stall forces, and only very rarely more than 2 (see Figure 21). Stall forces in the plus direction showed one major peak at ~5-7 pN, corresponding to a single kinesin motor. From these stall force histograms, we can assume that our beads generally have 1-2 dyneins and 1 kinesin simultaneously interacting with the microtubule. This is a reasonable number when compared to the number of motors that generally pull a single cargo within a cell. Various studies have found ~1-5 of each motor type attached to a single *in vivo* cargo*(65, 66).*

Section 3.2 *In Vivo* Comparison

Our *in vitro* assay shows that there is no requirement for a regulatory protein in order to achieve saltatory motion. To further assess if the saltatory motion seen in our *in vitro* assay is similar to that seen in live cells, we observed the motion of lipid droplets inside human epithelial cells (A549 cells). We picked lipid droplets that were separated spatially from nearby droplets (so that they could be properly analyzed with the same computer program with which we analyzed the bead data and so that the environment during the observed motion was less crowded and more like that of our *in vitro* system.) We then analyzed the motion of these droplets using the same techniques described above, and compared the results to our *in vitro* data. We found that these lipid droplets exhibited similar behavior to our *in vitro* beads, although the frequency of >500nm reversals per 50 second trace was actually somewhat lower *in vivo* (11%) than *in vitro* (21%) (see Figures 22-24). However, we noticed that in crowded sections of the cells, the lipid droplets underwent more frequent reversals due to collisions with other lipid droplets. These areas were difficult to analyze quantitatively, however, since their crowded nature made it impossible to use our analysis program. The lower percentage of traces with reversals could be explained as an under-estimate of the actual number of reversals occurring in the cell, since the majority of reversals seemed to occur in crowded areas. Additionally, the cell could be actively regulating the outcome of the tug-of-war (in this case, inhibiting reversals) through some mechanism that would alter the motors' individual characteristics (for instance, phosphorylation of one type of motor creating a higher microtubule binding rate.) Other studies*(65, 66)* have measured much higher

frequencies of reversals in *in vivo* organelles—30-80% exhibited bidirectional motion (although their definitions of bidirectional motion differed somewhat from our own.)

Section 3.3 Effects of Altering Motor Ratios

Next we considered how changing the ratio of kinesin to dynein would alter the outcome of the tug-of-war. We repeated the experiment over a number of different kinesin:dynein ratios. In one series of experiments we held the amount of kinesin constant and varied the amount of dynein added, while in a second series of experiments we held the dynein concentration constant and varied the dilution of the kinesin added. Figure 25 shows the resulting histograms (for varying kinesin concentrations) of net distance traveled for each kinesin:dynein ratio. Surprisingly, the histograms show vary little variation across a wide range of kinesin:dynein ratios, in both the case of varying the dynein amount and the case of varying the kinesin amount. Histograms of the average velocity of each roughly-constant-velocity segment show slightly more of a shift with the variation of kinesin:dynein ratio (see Figure 26), but the shift is still more subtle than might be expected. Repeating the experiment with a constant kinesin concentration while varying the dynein concentration showed similar results (see Figures 27-28). According to the Lipowsky tug-of-war model, the results of the motors' tug-of-war should be very sensitive to changes in the motor ratio. The lack of a clear shift with motor ratio in our data indicates that our data are not entirely compatible with the Lipowsky model.

Section 3.4 Encountering and Bypassing Obstacles

We observed beads with kinesin and dynein attached encounter various types of obstacles. Two beads on the same microtubule often collided with one another (with either both moving or, more commonly, one stuck and one moving). We compared the collisions that occurred with beads that had both dynein and kinesin motors on them to beads that had only one or the other (see Figure 29). Beads with only kinesin attached generally disassociated from the microtubule upon collision with another bead. Beads with only dynein most often became stuck in place next to the other bead, although they sometimes reversed direction upon collision. In contrast, beads with both motors most often reversed direction after colliding with another bead.

We also observed beads encountering an intersection with another microtubule. Depending on which microtubule was on top, one would expect that this situation would sometimes create an obstacle for the motors. In many cases, the beads simply passed through or switched microtubules. Beads with both motors sometimes reversed direction upon encountering a microtubule intersection, and in rare cases reversed direction twice, successfully passing through the intersection on the second try (see Figure 30).

To create a more physiologically relevant scenario, we bound the 4RL isoform of the tau MAP protein to microtubules and observed the beads interacting with these obstacles. Tau protein forms patches of several tau proteins clustered together when mixed with microtubules at sufficient concentrations*(5, 6)*. Tau has been shown to cause kinesin molecules to detach from the microtubule, while dynein molecules are likely to reverse direction upon encountering a patch of tau*(5)*. We observed beads with dynein and

kinesin often reversed direction upon encountering tau patches (Figures 31-32). Interestingly, in some cases the multiple reversals of the beads eventually led to successfully bypassing the tau patch obstacle (see Figure 31).

Section 3.5 Yeast Dynein Experiments

We also tested what effect replacing mammalian dynein with yeast dynein would have on our assays. Yeast dynein has several important differences from mammalian dynein: it has a much larger stall force (~7-8 pN, more on par with kinesin's stall force) and has a ~10x slower velocity than mammalian dynein. In addition, yeast dynein does not undergo frequent backwards-directed motion unless under large backward load. Yeast dynein is not known to be involved in the transport of organelles inside yeast cells*(42)*—rather, it is involved with chromosome segregation and mitotic spindle orientation*(76)*. If the propensity for mammalian dynein to walk backwards is indeed important for saltatory motion to occur, one would expect assays using yeast dynein to have significantly different results.

In experiments using truncated yeast dynein rather than full-length mammalian dynein (along with a truncated kinesin construct), we found that reversal events were extremely rare. Although we are not able to rule out the possibility that the truncation of the yeast dynein contributed to its inability to generate saltatory motion *in vitro*, it is possible that the fact that yeast dynein does not walk backwards easily could be an important factor in why it does not exhibit saltatory motion when combined with truncated kinesin. (See Chapter 4:Discussion for a more in-depth discussion on this topic.)

Section 3.6 Optical Trap "Snap-Back" Experiments

As described above, experiments using truncated yeast dynein suggested that mammalian dynein's ability to step backwards is crucial to achieving saltatory motion. Based on this finding, we hypothesized that dynein does not always detach during + directed motion but rather walks backwards *with* kinesin at least some of the time. To test this idea, we devised an optical trap experiment in which we simulated a kinesin molecule walking in 8 nm steps and pulling backwards on kinesin. (See Chapter 2:Materials and Methods). To do this, we trapped a bead with only one type of motor in the optical trap and brought it into contact with a microtubule on a coverslip. Then, we stepped the piezo stage (upon which the coverslip was sitting) backwards in 8 nm steps and observed the behavior of the motor. In the case of a "normal" motor such as kinesin, which only takes slow backwards steps when under super-stall forces*(77, 78)*, one would expect the motor to stay attached to the microtubule until the stepping of the piezo stage creates a force that is close to the motor's stall force, at which time the motor would let go of the microtubule, causing the bead to "snap back" to the center of the trap in a single clean step (see Figure 33).

3.6.1 Kinesin Snaps Back

When we performed this experiment with kinesin-only beads, this is essentially what we saw (see Figure 34). Beads with kinesin occasionally took slow backwards steps, but mostly stayed attached to the microtubule until the stall force was reached, after which the bead snapped back to center.

3.6.2 Mammalian Dynein Walks Back

Beads with dynein motors, on the other hand, behaved quite differently. Although they sometimes snapped back as did kinesin-only beads, the frequently exhibited a different behavior in which the dynein took rapid, large backwards steps rather than detaching from the microtubule (see Figure 35). These large steps are consistent with dynein's flexible nature and ability to take large steps. The data do seem to indicate that dynein, at least some of the time, walks backwards with the opposing motor rather than detaching from the microtubule when pulled backwards. This is a detail not included in the Lipowsky model, which assumes that motors only take slow backward steps when under super-stall forces.

3.6.1 Yeast Dynein Snaps Back

To further test this idea, we repeated this optical trap experiment using yeast dynein in the place of mammalian dynein. If our hypothesis is correct, we would expect yeast dynein to "snap-back" rather than walk back as mammalian dynein does. Indeed, yeast dynein did not exhibit rapid backwards stepping in our piezo step-back assay (Figure 36). Instead it behaved more like kinesin motors, taking some slow backward steps and eventually snapping back as the motor completely let go of the microtubule after its stall force was exceeded. Apparently, yeast dynein holds on more tenaciously to the microtubule does than mammalian dynein, and it does not walk as readily backward with an opposing motor. This is consistent with our hypothesis that the ability of mammalian

dynein to walk backwards with kinesin rather than detaching from the microtubule is indeed a crucial element in achieving saltatory motion.

A quantitative comparison of the frequency of "snap-back" events for kinesin, mammalian dynein, and yeast dynein was also completed (see Figure 37). Optical trap traces were fit using Student's T-test. Traces were then scored as having a "snap-back" event if the T-test fit had at least one step with a size larger than a given threshold limit. Threshold limits were set at 50 nm, 75 nm, or 100 nm. (It was assumed that a step of this magnitude indicated a full release from the microtubule rather than an actual motor step.) Mammalian dynein traces showed significantly less snap-back events at all threshold limits, indicating that this motor type was more likely to take backward steps but remain engaged with the microtubule rather than releasing.

Chapter 4: Discussion

Section 4.1 Modified Tug-of-war Model

As explained above, our results certainly support a tug-of-war model over a coordinated motion model. Since we did not include any sort of coordination complex in our *in vitro* system, we can be certain that such a regulatory system is not necessarily required to achieve saltatory motion. However, our data was also not entirely consistent with the simple tug-of-war as presented in the Lipowsky model. We found that outcome of the tug-of-war did not seem to be very sensitive to the ratio of kinesin:dynein which we added to our beads. In addition, the Lipowsky model does not account for dynein's tendency to walk backwards when pulled back by an opposing motor, or indeed, even when not under any external load at all. Finally, it is not readily obvious based on the Lipowsky model why beads so often reverse direction upon encountering obstacles.

We therefore present a modified tug-of-war model, as can be seen in Figure 38. The main difference between this model and the Lipowsky model is the idea that dynein stays attached to the microtubule and walks backwards with kinesin (towards the + end) rather than detaching completely when kinesin is "winning". This model also explains why cargoes are more likely to reverse directions after collisions and provides insight into how cargoes can successfully navigate around the significantly crowded cellular environment.

In our modified tug-of-war model, shown in detail in Figure 39, the cargo is first being carried in the + end direction by kinesin (Figure 39A). However, the dynein motors are

also attached to the microtubule and are walking backwards *with* kinesin. The cargo then encounters some sort of an obstacle, such as a microtubule associated protein, at which time the kinesin lets go of the microtubule and dissociates (which is what we found kinesin motors most likely to do when encountering obstacles), as seen in Figure 39B. Since the dynein motors are still attached to the microtubule and ready to take over, the cargo then reverses direction and heads in the – end direction. Since dynein sometimes takes off-axis steps from one protofilament to another, it is possible for it to wander to a different protofilament during this time (Figure 39C). At some point, the kinesin motors reattach, and the cargo again moves in the + direction, although on a new protofilament which is not blocked by the obstacle (Figure 39D). Thus, dynein's unique abilities to walk backwards and to change protofilaments have enabled the cargo to successfully bypass an obstacle without detaching from the microtubule.

Chapter 5: Conclusions

Section 5.1 Tug-of-war and Dynein's Role

These results support a tug-of-war model over a coordinated motion model; they show conclusively that no mediating proteins or coordination complex is required to achieve saltatory motion. However, although our data indicate that external coordination factors are not required to facilitate the back-and-forth motion of cargos within cells, a simple tug-of-war model in which the two motors are considered to be equivalent except in directionality is also not entirely complete. It is, in fact, *too* simplified. The added complexity needed to explain saltatory motion is found within the dynein motor itself. Dynein's ability to walk bidirectionally is fundamentally important to a cargo's back-and-forth motion. In addition, dynein's flexibility, ability to switch from one protofilament to another as it walks, and bidirectionality are all fundamentally important to the cell's ability to maneuver cargos within a densely packed environment full of obstacles and road blocks. Dynein's role as an accommodating tug-of-war partner could be all that is necessary to explain saltatory motion as seen *in vivo*.

Section 5.2 Future Work

Future work will include studying different types of kinesin or dynein motors (for instance, variations of kinesin which have lower stall forces) to see how this affects the outcome of the tug-of-war. A full-length yeast construct (rather than the truncated yeast construct used here) will also be used to verify that the lack of saltatory motion observed with this type of dynein was not simply due to the shorter stalk length.

Finally, it would be most helpful and interesting to be able to devise a system in which the exact number and type of motors that are simultaneously interacting with the microtubule for a give cargo at a given time could be unambiguously determined. Future work could include efforts to create such a system.

Figures

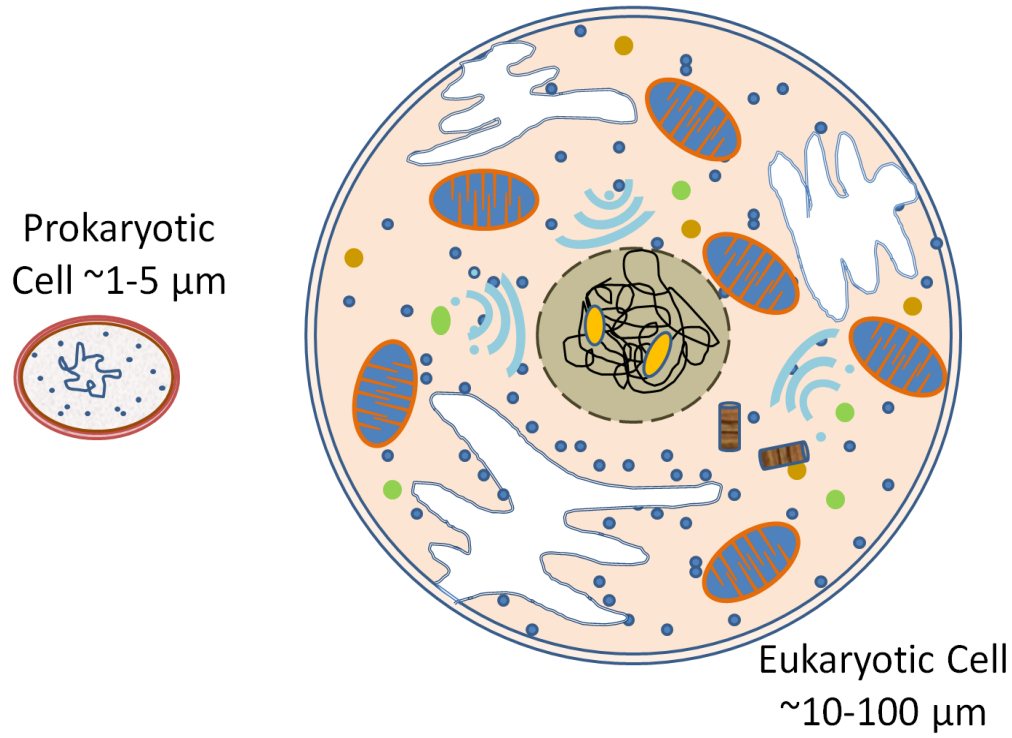

Figure 1. Cartoon Depiction of Prokaryotic and Eukaryotic Cells. The prokaryotic cell (left) is much smaller (~1-5 µm) and simpler than the larger (10-100 µm) and more complex eukaryotic cell (right).

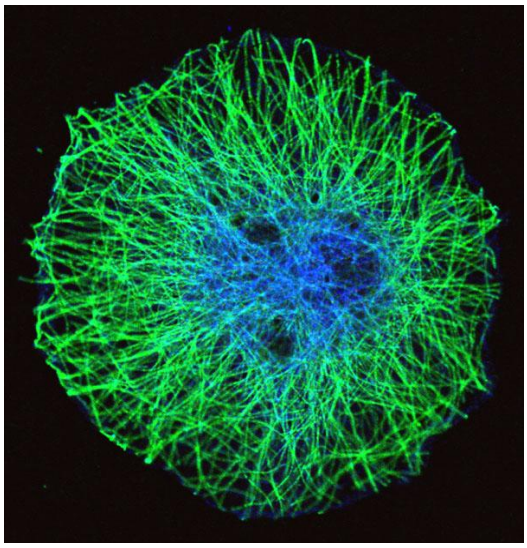

Figure 2. The Microtubule Network. A Drosophila (S2R+) cell is shown with its microtubules stained in green and its nucleus stained in blue. The microtubules generally extend radially outward from the nucleus to the cell membrane. The + end of the microtubules is near the outside of the cell (the cell membrane), while the – end of the microtubules is near the nucleus. Figure used by permission from Katja Roeper lab, http://www.pdn.cam.ac.uk/staff/roper/RoperLab/ImageGallery.html

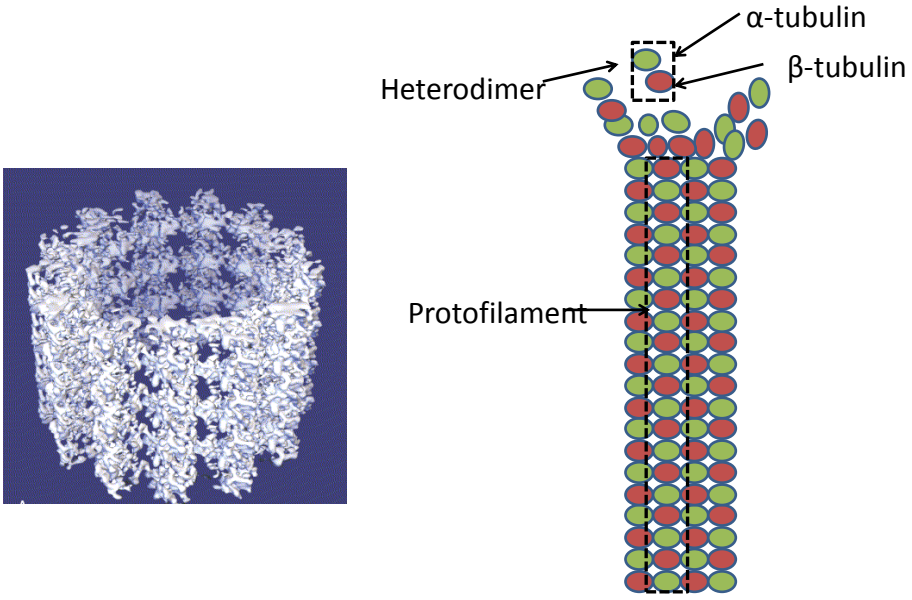

Figure 3. Microtubule Strucutre. (Left) A model of a segment of microtubule derived from cryo-electron microscopy. The + end is at the top of the image. Figure used by permission from Downing, 2002*(79)*. (Right) Cartoon depiction of microtubule structure, showing the polymer formed of alph-beta heterodimers. Protofilaments run vertically along the structure. A single protofilament is outlined (dashed box).

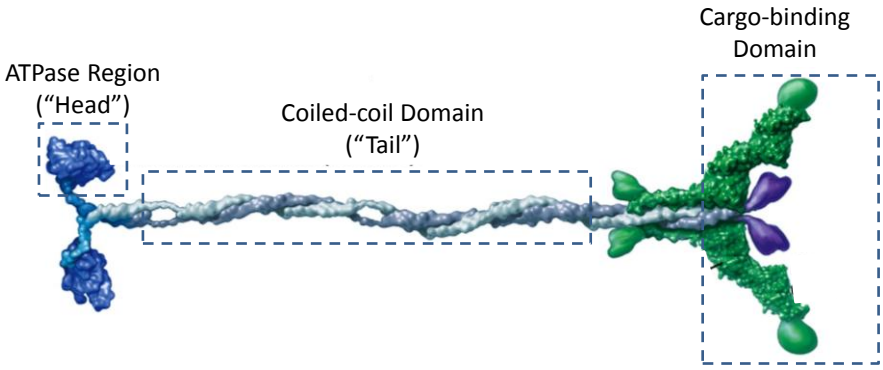

Figure 4. Kinesin Molecule Structure. A depiction of a kinesin motor protein, showing the two dimerized heavy chains and light chains. Various regions of the motor—the ATPase region, the coiled-coiled region, and the cargo binding domain--are outlined (dashed boxes). Figure used with permission (modified) from Vale, 2003*(80)*.

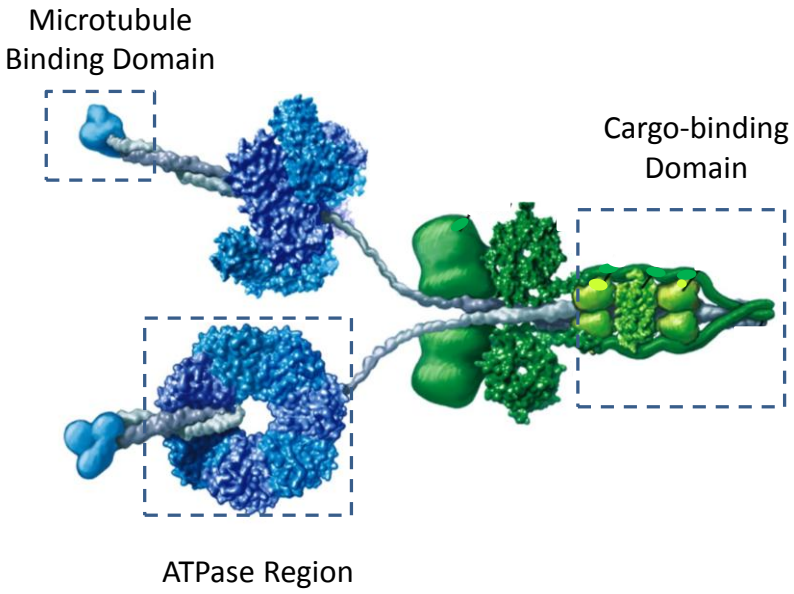

Figure 5. Dynein Molecule Structure. A depiction of a dynein motor protein, including the two dimerized heavy chains and various light and intermediate chains. Various regions of the motor—the ATPase region, the microtubule binding domain, and the cargo binding domain--are outlined (dashed boxes). Figure used with permission (modified) from Vale, 2003*(80)*.

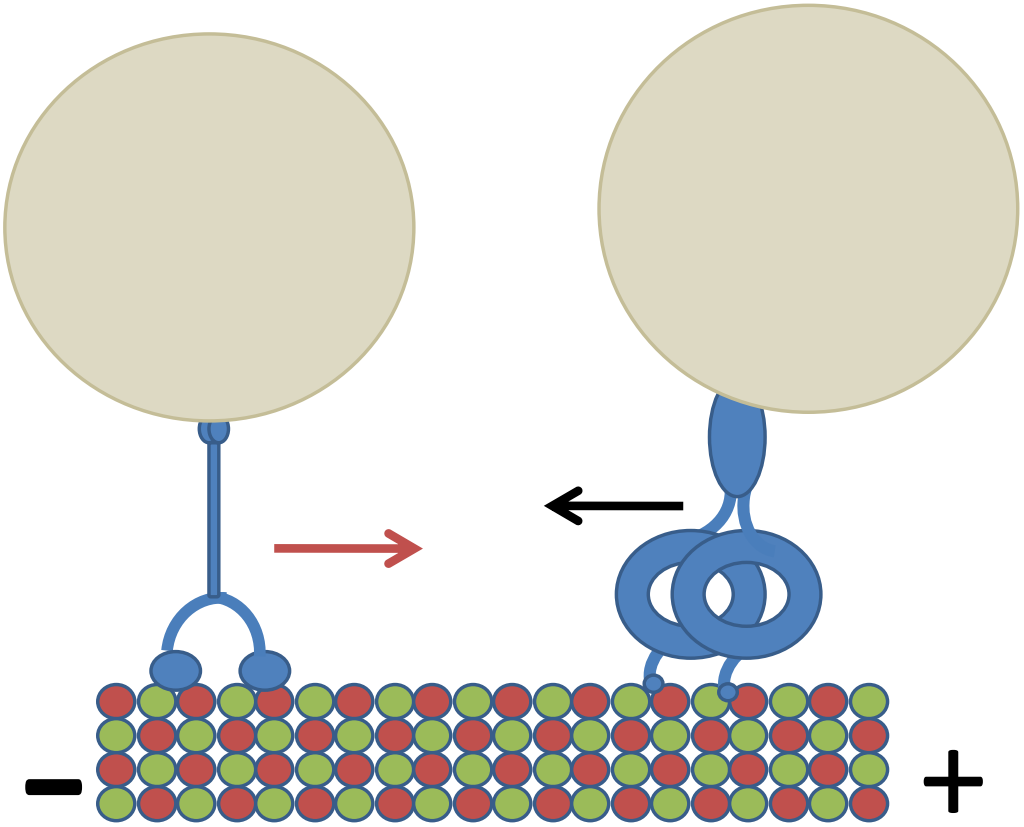

Figure 6. Cartoon Depiction of Motors with Cargos Bound. Kinesin (left) walks towards the + end of the microtubule, while dynein (right) walks towards the – end. A naïve assumption would be that cargos have one or the other type of motor attached, based on the intended direction of the destination

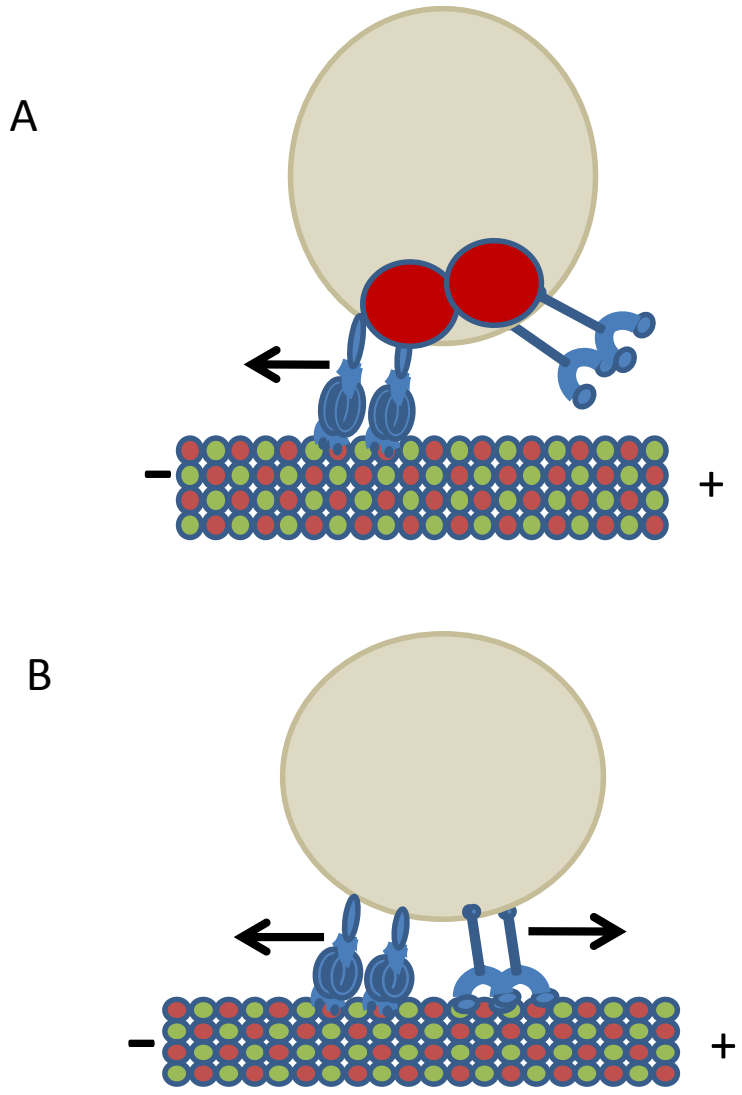

Figure 7. Two Competing Models for Saltatory Motion. (A) The coordinated motion model assumes that some accessory protein or complex regulates (depicted in red) when one motor is on and when one motor is off. The motors are never competing—that is, they are never simultaneously bound to the microtubule. (B) The tug-of-war model assumes that there is no coordinating complex, but rather the motion is governed by a simple battle between motors. The "winning" side (whether due to a higher stall force per motor or higher number of motors bound) determines the direction of motion, and motors of both type are competing by pulling against each other.

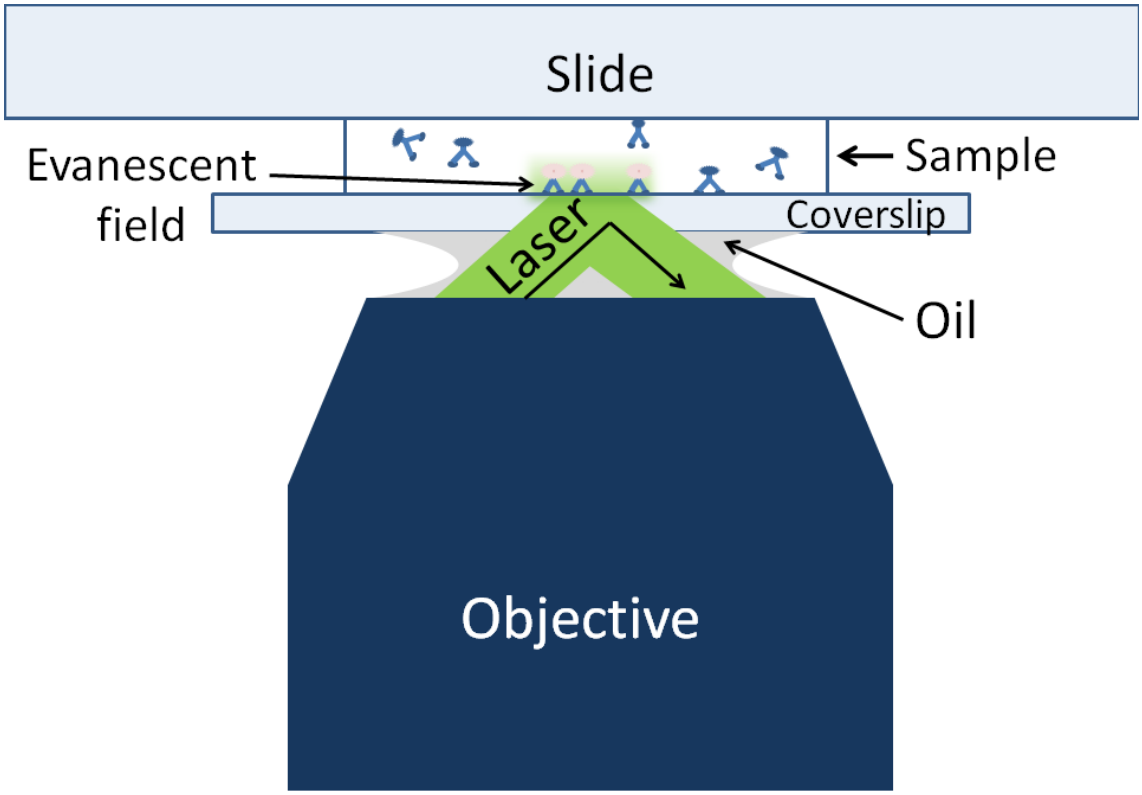

Figure 8. TIRF Microscopy. When the incoming laser is at the correct critical angle for its wavelength, it is totally reflected by at the glass/water interface, and only an evanescent field penetrates into the sample. This evanescent field loses half of its intensity every ~50nm into the sample, so effectively only flourophores within ~100m of the coverslip will be excited. This greatly minimizes background signal and will not photobleach dyes in the bulk of the sample. The oil between the sample chamber and the objective has the same index of refraction as the glass, and eliminates refraction of the laser which would occur if the laser traveled through air.

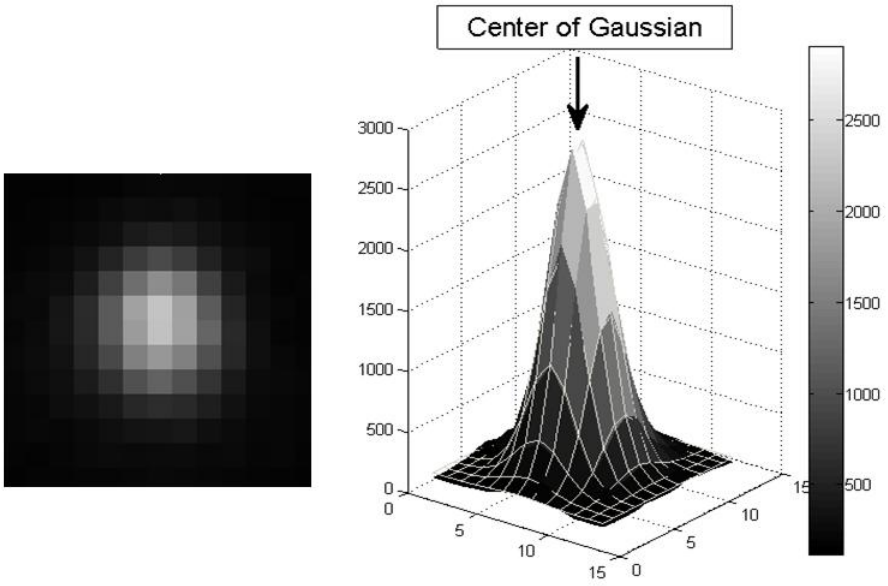

Figure 9. FIONA. Example of a cropped fluorophore point-spread function captured with a CCD camera (left), and the same point-spread function is plotted in three dimensions, intensity as a function of (x,y).. A Gaussian function is fitted to the PSF, shown as a mesh overlay in the plot. The center of the Gaussian can then be determined with a high level of accuracy (~1 nm).

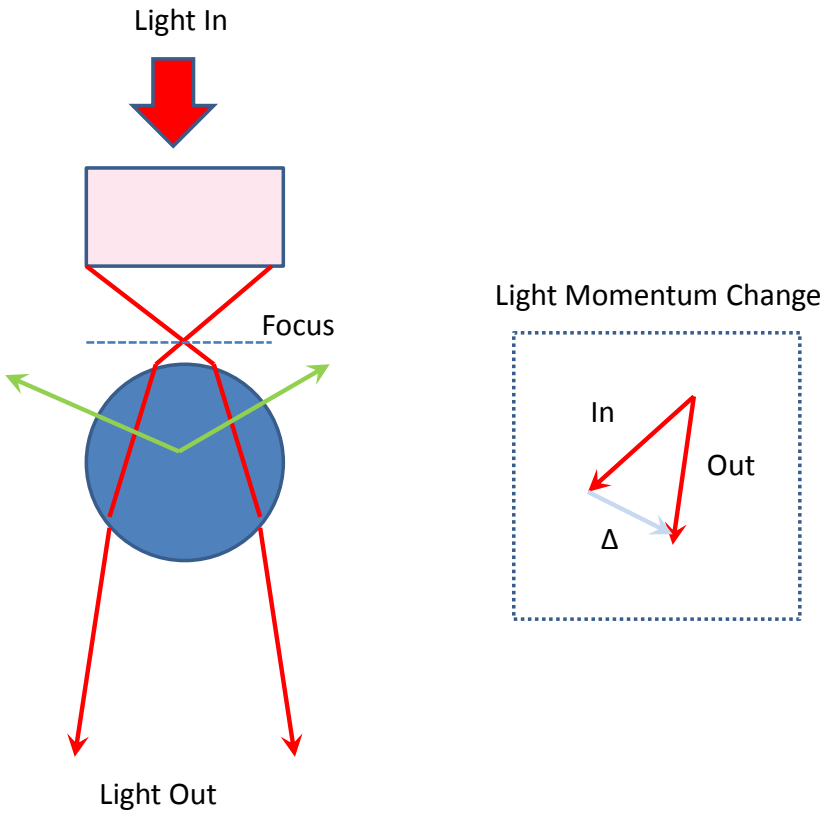

Figure 10. Optical Trap. A simplified ray diagram illustrating how an optical trap functions. A spherical particle sits just below the focus of a laser beam. Two representative light rays are depicted in red, showing how they are bent due to the refraction of the light as it passes through the transparent sphere. The resulting change in momentum for one of the beams is shown in the inset. An equal and opposite force to this change in momentum is applied to the sphere (green arrows), causing a net upward force that pushes the bead back towards the focus.

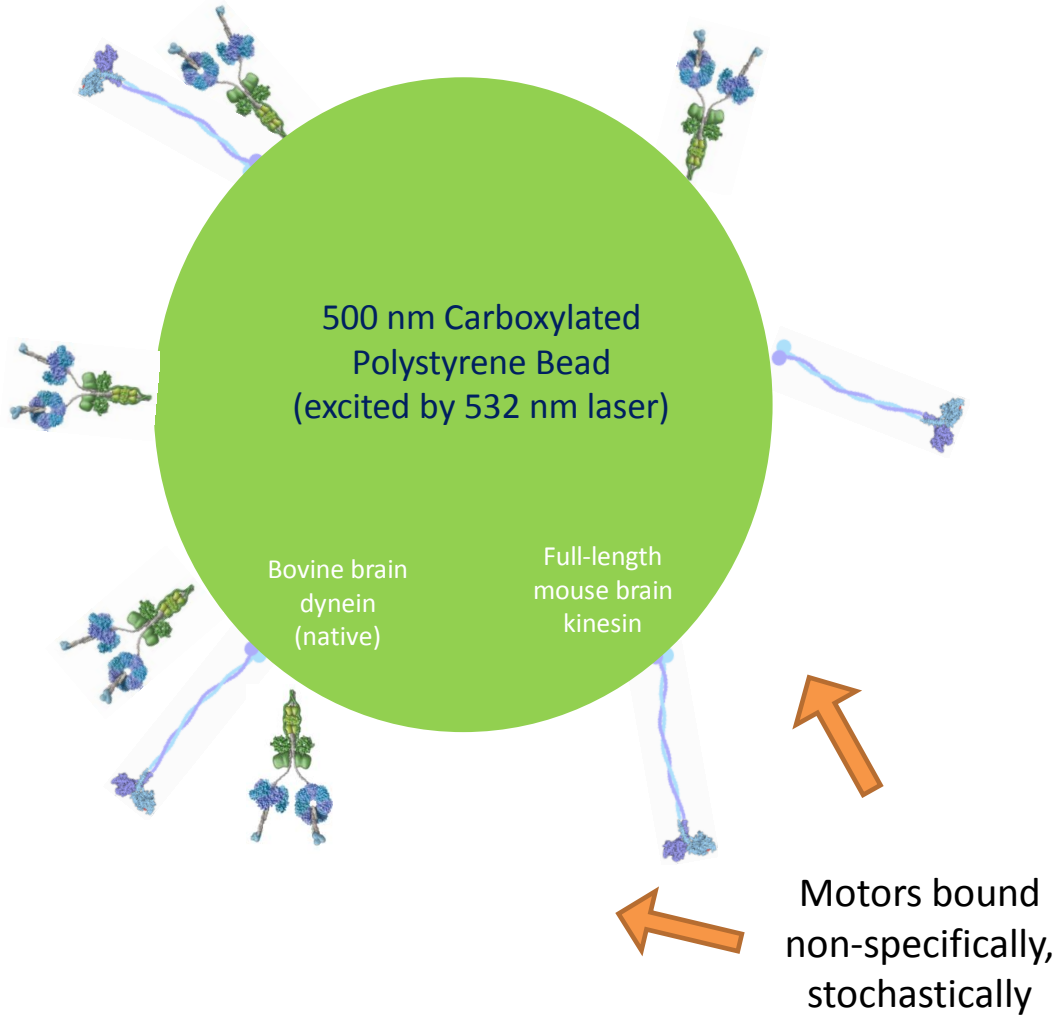

Figure 11. Fluorescent Bead Sample. Dynein and kinesin motors are non-specifically bound to a 500 nm diameter red (excited by 532 nm laser) carboxylated polystyrene bead. Motors are bound stochastically on the surface of the bead.

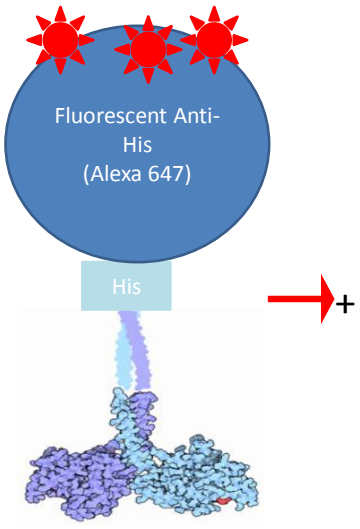

Figure 12. "Reference Kinesin" Sample. A truncated kinesin construct with a histidine tag is bound to a fluorescent anti-His antibody. This reference kinesin can then be used to distinguish the + end of the microtubule.

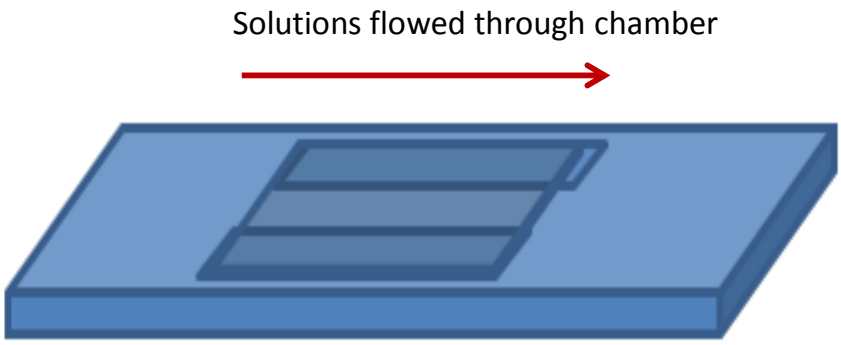

Figure 13. Flow Chamber**. Schematic of capillary flow chamber. The coverslip is attached using double-sided tape, leaving a thin chamber between the tape. Solutions are flowed through the chamber from one end using capillary action**

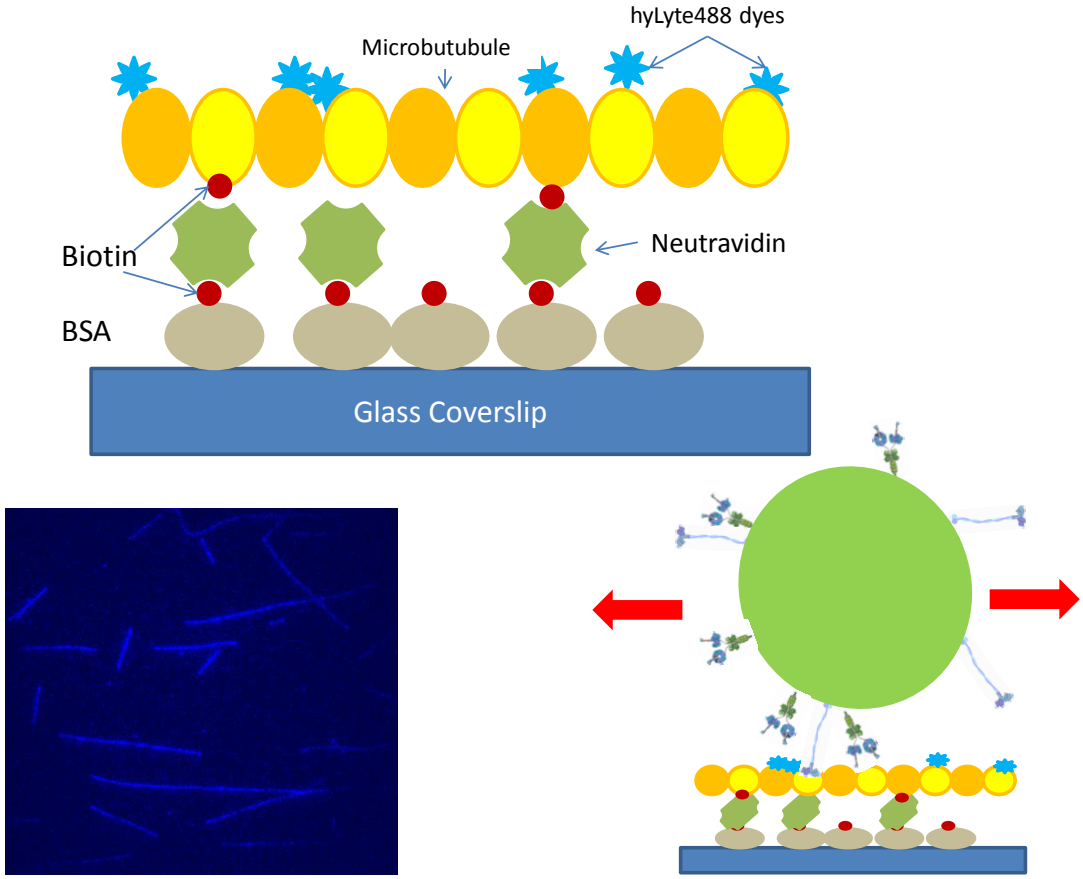

Figure 14. Experimental Setup. (Top) **Cartoon depiction of the experimental setup inside the flow chamber. Each "layer" is flowed through the chamber in succession. First BSA-biotin is attached to the glass coverslip. Neutravidin molecules are then bound to the biotin on the BSA-biotin. Biotinylated fluorescent microtubules are then bound to the neutravidin. These can be imaged by exciting the fluorophores on the microtubules (see example image,** bottom left**). Finally, the bead sample is flowed through and the motors can walk on the microtubules** (bottom right)**.**

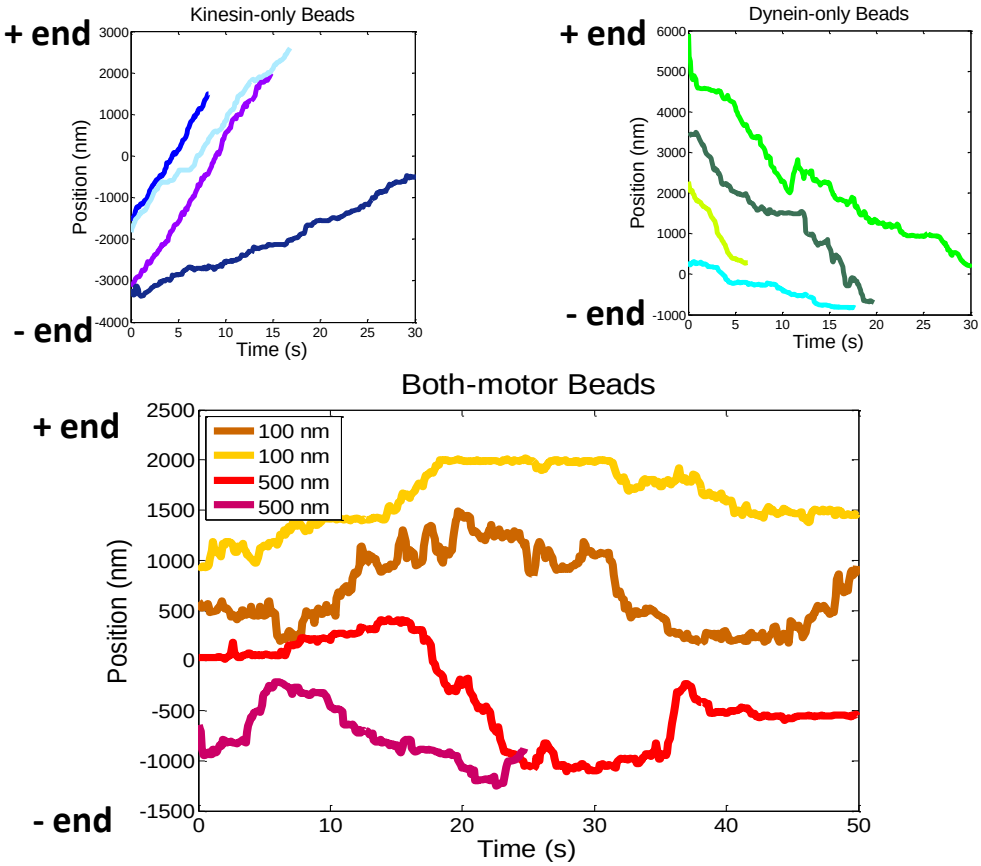

Figure 15. Results of I*n Vitro* Tug-of-War Fluorescence Assay. Position versus time for motors carrying beads on microtubules driven by 2 mM [ATP]. Traces are 50 seconds in length, or as long as the bead remained within the field of view. (Left) Example traces of 500 nm beads with kinesin-only walking in the plus direction. (Center) Example traces of 500 nm beads with dynein-only, walking in the minus direction. (Right) Example traces of beads with both dynein and kinesin exhibiting bidirectional saltatory motion. The top two traces show 100 nm beads with both motors attached, while the bottom two traces are from 500 nm beads. Similar behavior was observed for both 100 nm and 500 nm beads.

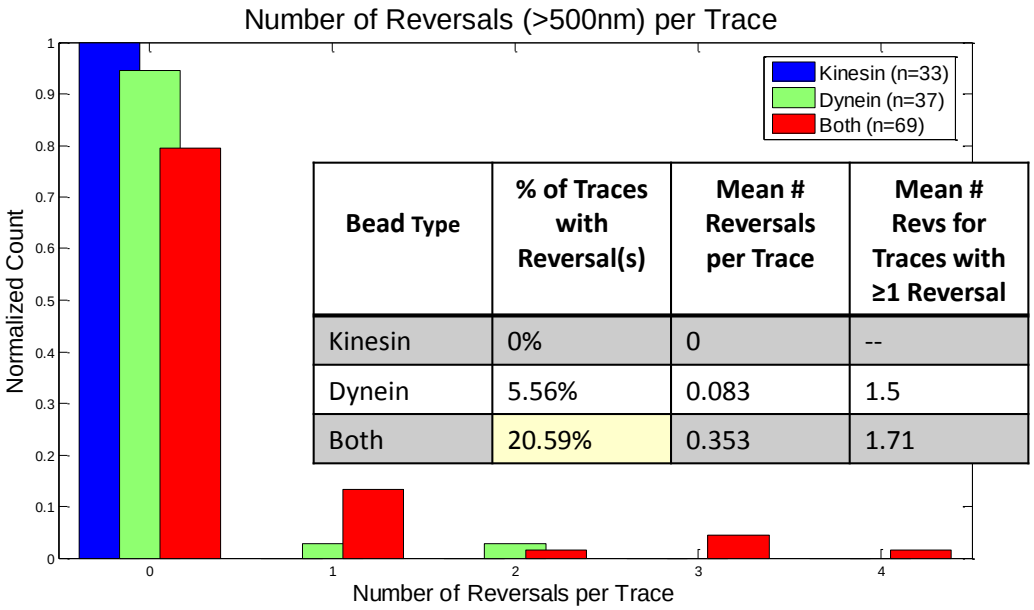

Bead Type	% of Traces with Reversal(s)	Mean # Reversals per Trace	Mean # Revs for Traces with ≥1 Reversal
Kinesin	0%	0	--
Dynein	5.56%	0.083	1.5
Both	20.59%	0.353	1.71

Figure 16. Evidence of Saltatory Motion. Histogram showing the number of reversals with >500 nm run lengths before and after the reversal per trace for beads with kinesin-only (blue), dynein-only (green), and both motors (red). Beads with both motors were much more likely to have direction reversals than beads with dynein or kinesin alone (21% compared to 5% or 0%, respectively).

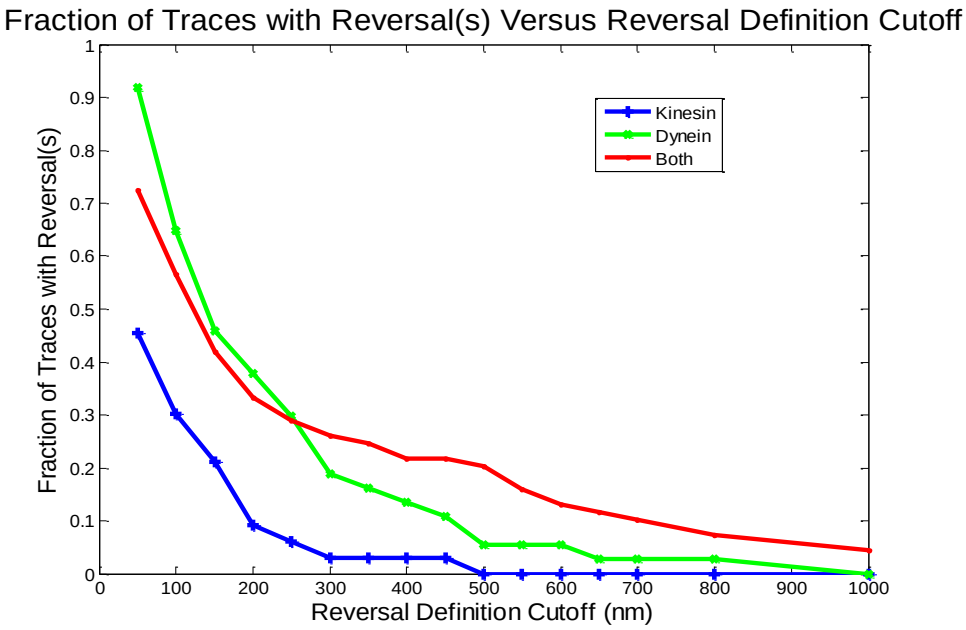

Figure 17. Additional Analysis of Saltatory Motion. The fraction of traces (50 seconds, or as long as the bead remained in the field of view) which exhibited at least one reversal versus the threshold segment length (*i.e.* distance of runs in each direction before and after a reversal point) used to define a reversal event. Although dynein-only beads have frequent reversals with smaller threshold values, beads with both motors clearly have more reversals with larger segment lengths (*i.e.* ≥ 500 nm in each direction before and after reversal).

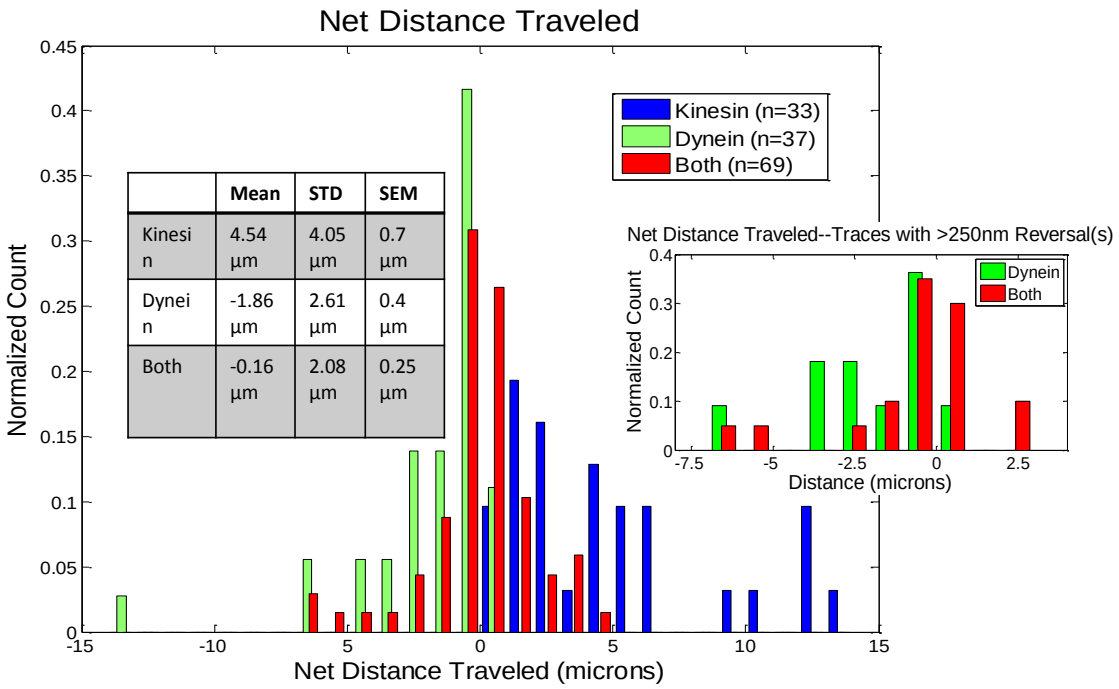

Figure 18. Net Distance Traveled per Trace. Histogram of net distance traveled per trace for beads with kinesin-only (blue), dynein-only (green), or both motors (blue). The three types of beads clearly have different net distance distributions. (Inset) The subset of traces exhibiting at least one ≥ 250 nm reversal, again showing beads with both dynein and kinesin had a significantly different net distance traveled than beads with dynein only even within this subset. This effectively excludes any beads in the kinesin-and-dynein sample that were more likely to have *only* kinesin or only dynein attached to that particular bead, thus excluding any effect due to simple averaging of the results of dynein-only and kinesin-only beads. The dynein-and-kinesin sample shows a distinct characteristic that can only come from the interplay of dynein and kinesin on a single bead.

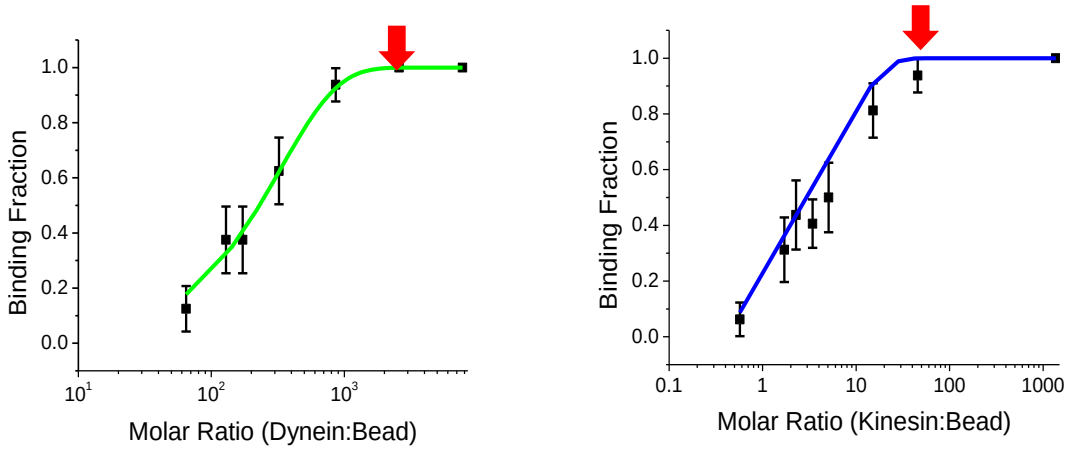

Figure 19. Analysis of the Number of Motors Engaged per Bead. The fraction of beads bound to axoneme as a function of relative motor concentration. Beads were held in the optical trap for 30 seconds over an axoneme in order to allow them to bind (n≥15 for each data point). The fraction of beads that bound to the axoneme was recorded and plotted versus relative motor concentration. The data was fit to 1-exp(-λf), the Poissonian probability that one or more kinesin molecules are bound to a bead*(20)*. Error bars are $\pm p_m(1-p_m)/N^{1/2}$. Red arrows indicate the concentration of motors used in the fluorescence assay experiments.

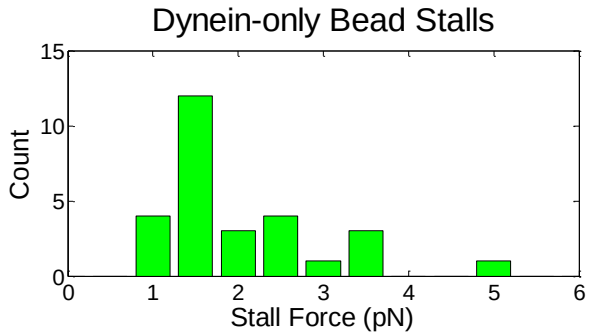

Figure 20. Stall Forces for Beads with Dynein-only. Stall force histogram for beads with dynein only (with the same dynein:bead ratio as was used in the fluorescence bead assays). Peaks at ~1-2 pN and ~3-4 pN indicate that 1-2 motors per bead were simultaneously interacting with the microtubule. Rarely, 3 motors were simultaneously engaged.

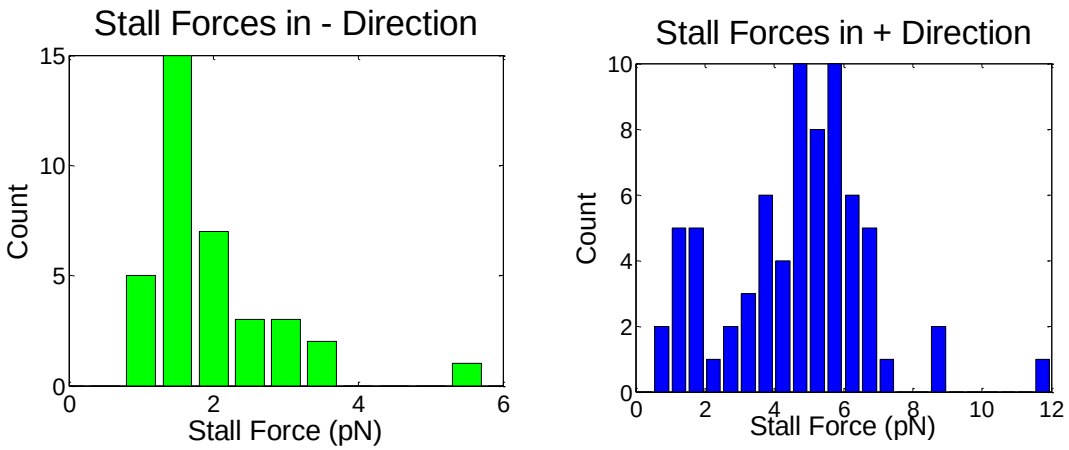

Figure 21. Stall Forces for Beads with Both Motors. Stall force histogram for beads with both dynein and kinesin dynein only (with the same dynein:bead and kinesin:bead ratios as were used in the fluorescence bead assays). Smaller (500 nm) kinesin-beads were used as a reference to designate the directionality of each axoneme. 1.2 µm beads with both motors were then brought into contact with the same axoneme and stall forces measured in each direction. Peaks in the – end direction at ~1-2 pN and ~3-4 pN indicate that 1-2 dynein motors per bead were simultaneously interacting with the microtubule. The single major peak at ~5-7 pN in the + end direction shows that a single kinesin was generally pulling the bead at a time. Thus, we conclude that our beads had, on average, ~1-2 dyneins and ~1 kinesin simultaneously interacting with the microtubule.

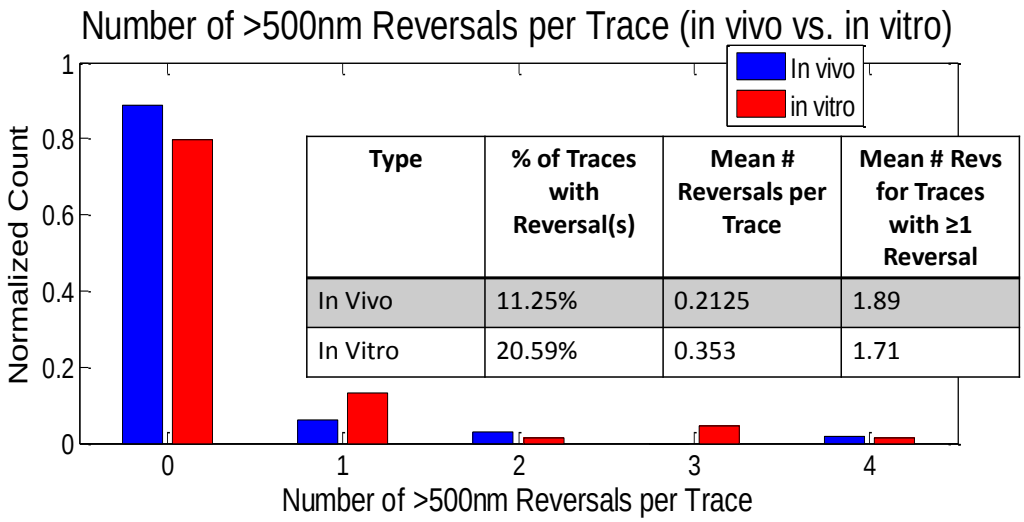

Type	% of Traces with Reversal(s)	Mean # Reversals per Trace	Mean # Revs for Traces with ≥1 Reversal
In Vivo	11.25%	0.2125	1.89
In Vitro	20.59%	0.353	1.71

Figure 22. ***In Vivo* versus *In Vitro* Comparison. Histogram showing the number of reversals with >500 nm run lengths before and after the reversal per trace for beads kinesin and dynein *in vitro* (red) and for lipid droplets *in vivo* (blue).**

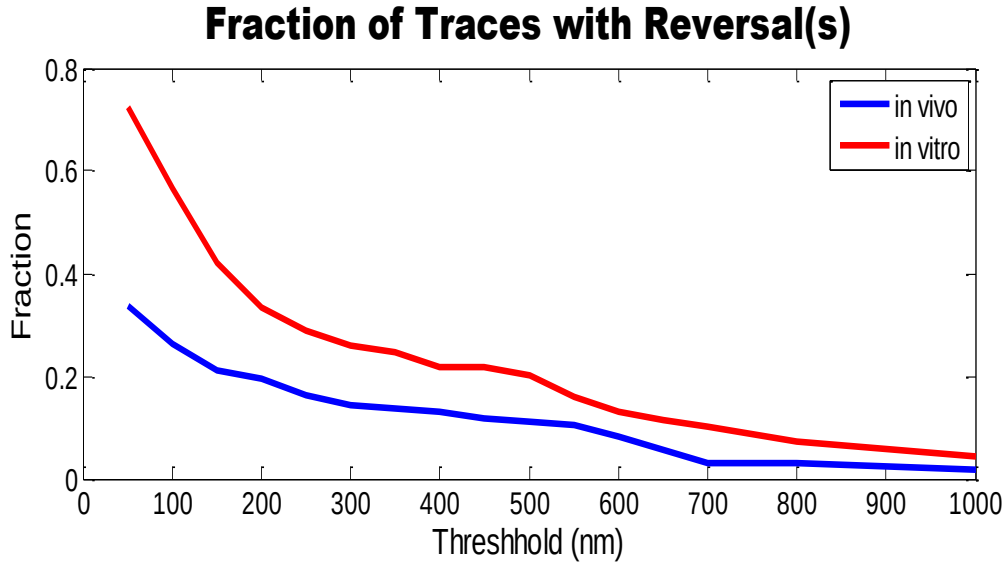

Figure 23. Fraction of Traces with Reversals for *In Vivo* versus *In Vitro*. The fraction of traces (50 seconds, or as long as the bead remained in the field of view) which exhibited at least one reversal versus the threshold segment length (*i.e.* distance of runs in each direction before and after a reversal point) used to define a reversal event for beads *in vitro* (red) and lipid droplets *in vivo* (blue).

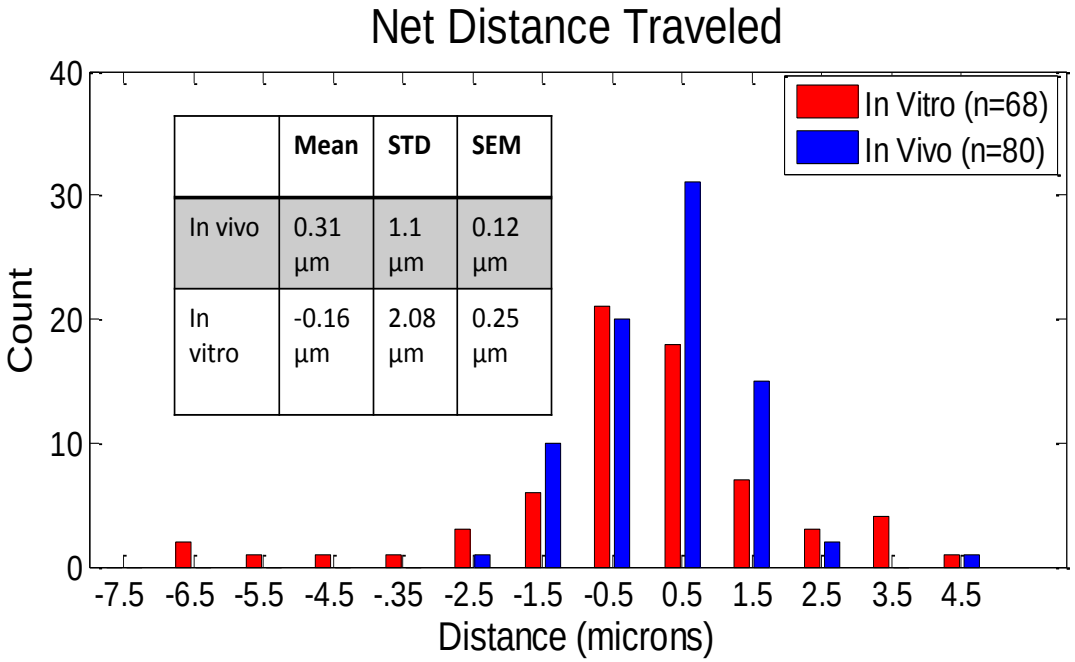

Figure 24. Net Distance Traveled for *In Vivo* versus *In Vitro*. Histogram of net distance traveled per trace for beads with kinesin and dynein *in vitro* (red) and for lipid droplets *in vivo* (blue). The net distance distributions for the two look quite similar, although the *in vivo* distribution was slightly more in the + direction (mean 0.31 µm compared to -0.16 µm for the *in vitro* traces).

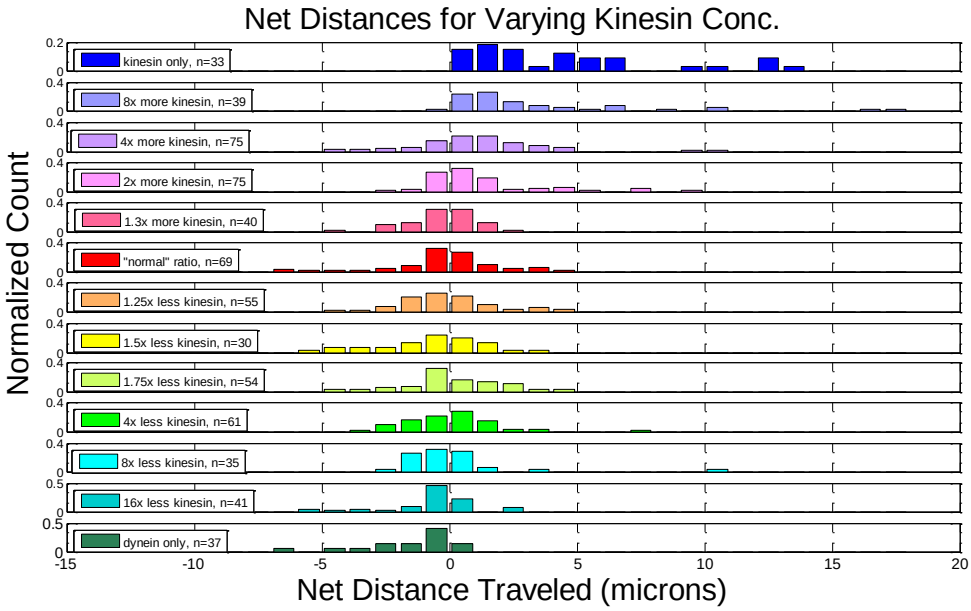

Figure 25. Net Distances for Varying Motor Ratios—Kinesin. Results of varying the ratio of kinesin:dynein added to the fluorescent beads. The dynein concentration was held constant (500 nM), while the relative amount of kinesin was varied. A histogram for net distance traveled for each kinesin:dynein ratio. The top histogram shows beads with kinesin only, and the bottom histogram shows beads with dynein only. Similar to what is seen in Figure 27, the net distance distribution varies surprisingly little over a wide range of kinesin:dynein ratios.

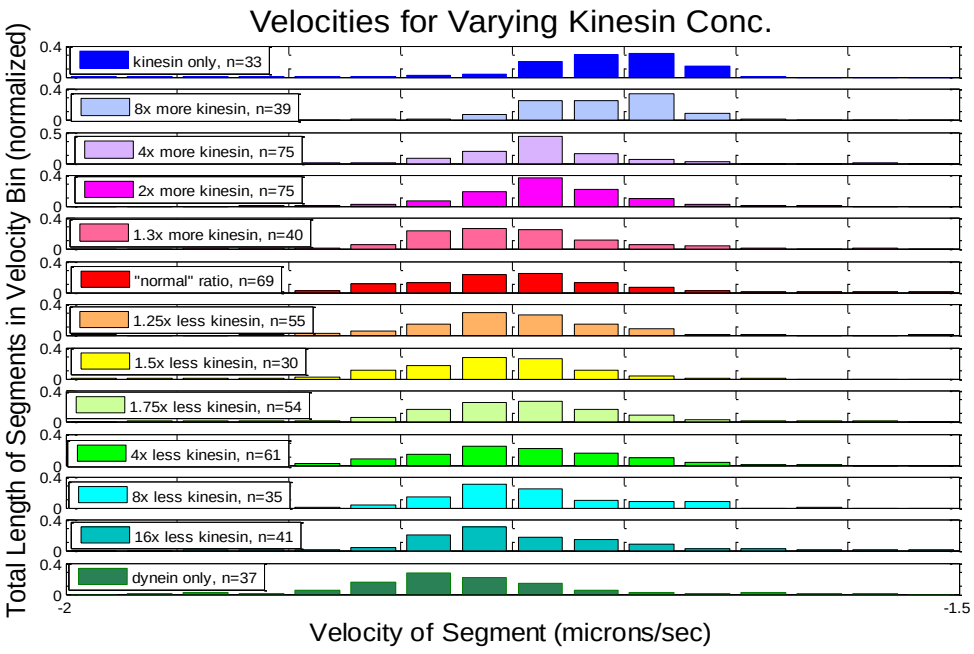

Figure 26. Velocities for Varying Motor Ratios—Kinesin. A histogram showing the average velocity for constant velocity segments of the traces for each kinesin:dynein ratio. (The y axis shows the total length of segments for each velocity bin, normalized). Again, the top histogram shows beads with kinesin only, and the bottom histogram shows beads with dynein only. Also similar to Supplementary Figure 6, the velocity distribution gradually shifts with the motor ratio.

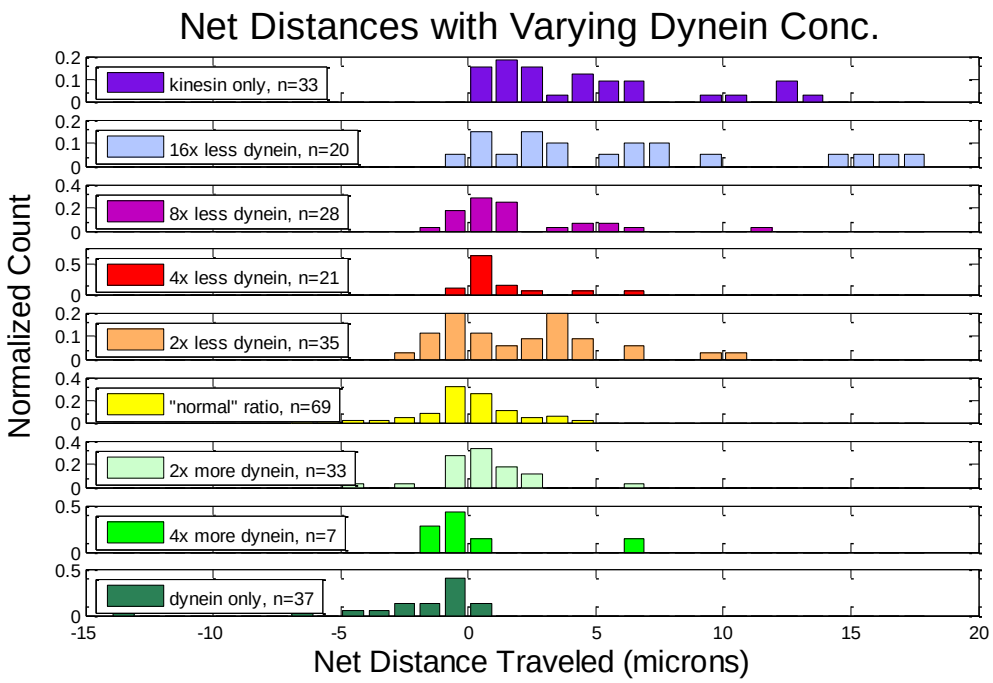

Figure 27. Net Distances for Varying Motor Ratios—Dynein. Results of varying the ratio of kinesin:dynein added to the fluorescent beads. The kinesin concentration was held constant (6.6 nM), while the relative amount of dynein was varied. A histogram for net distance traveled for each kinesin:dynein ratio. The top histogram shows beads with kinesin only, and the bottom histogram shows beads with dynein only. The net distance distribution varies surprisingly little over a wide range of dynein:kinesin ratios.

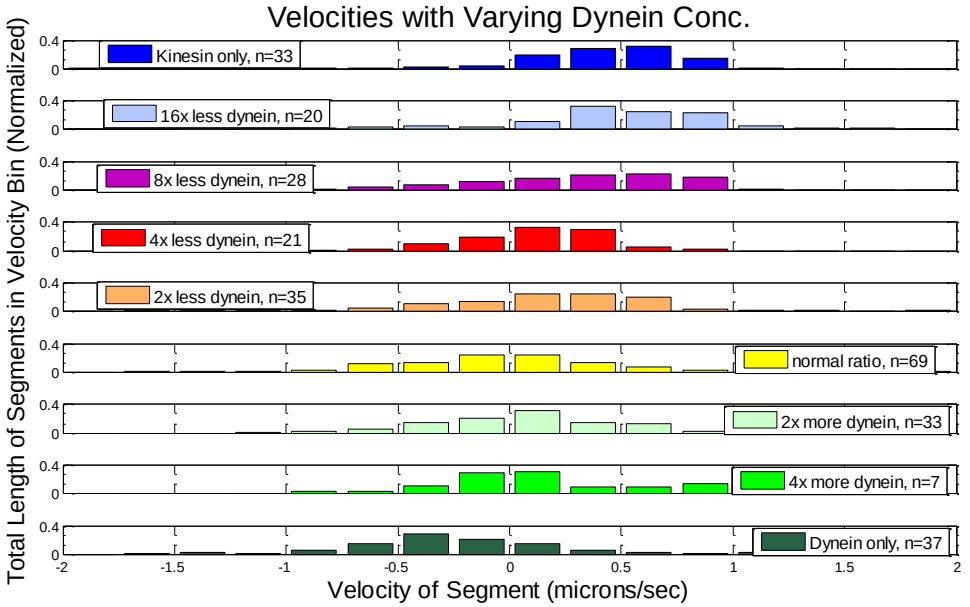

Figure 28. Velocities for Varying Motor Ratios—Dynein. A histogram showing the average velocity for constant velocity segments of the traces for each kinesin:dynein ratio. (The y axis shows the total length of segments for each velocity bin, normalized). Again, the top histogram shows beads with kinesin only, and the bottom histogram shows beads with dynein only. The velocity distribution shifts slightly with the motor ratio, although still less than expected.

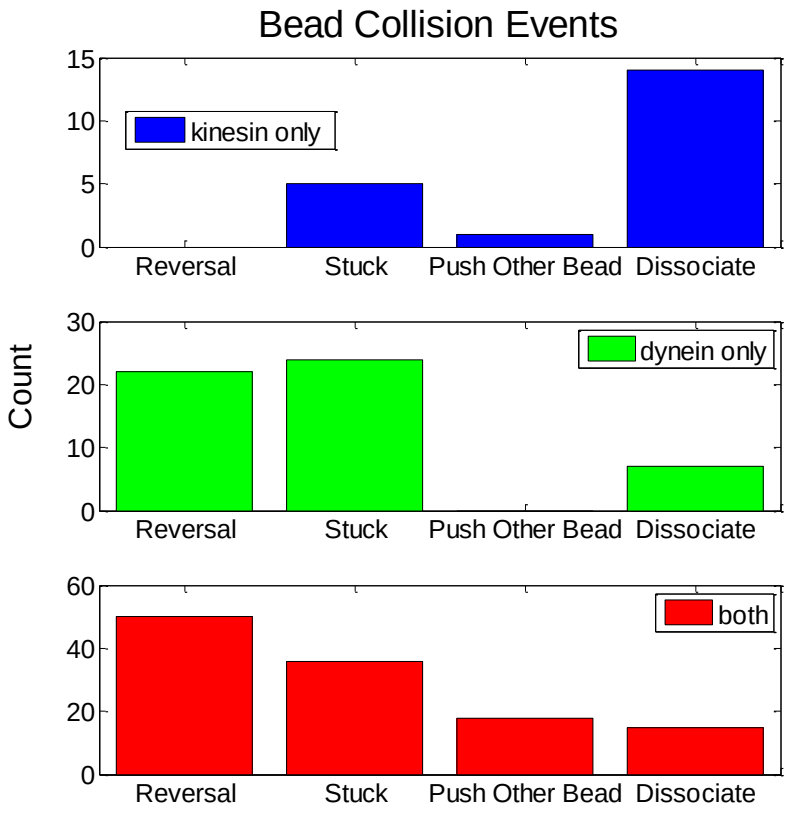

Figure 29. Results of Motors Encountering Other Beads. The outcome of bead collision events for beads with kinesin-only (blue), dynein-only (green), or both motors (red). Beads with both motors were more likely to reverse directions upon colliding with another bead.

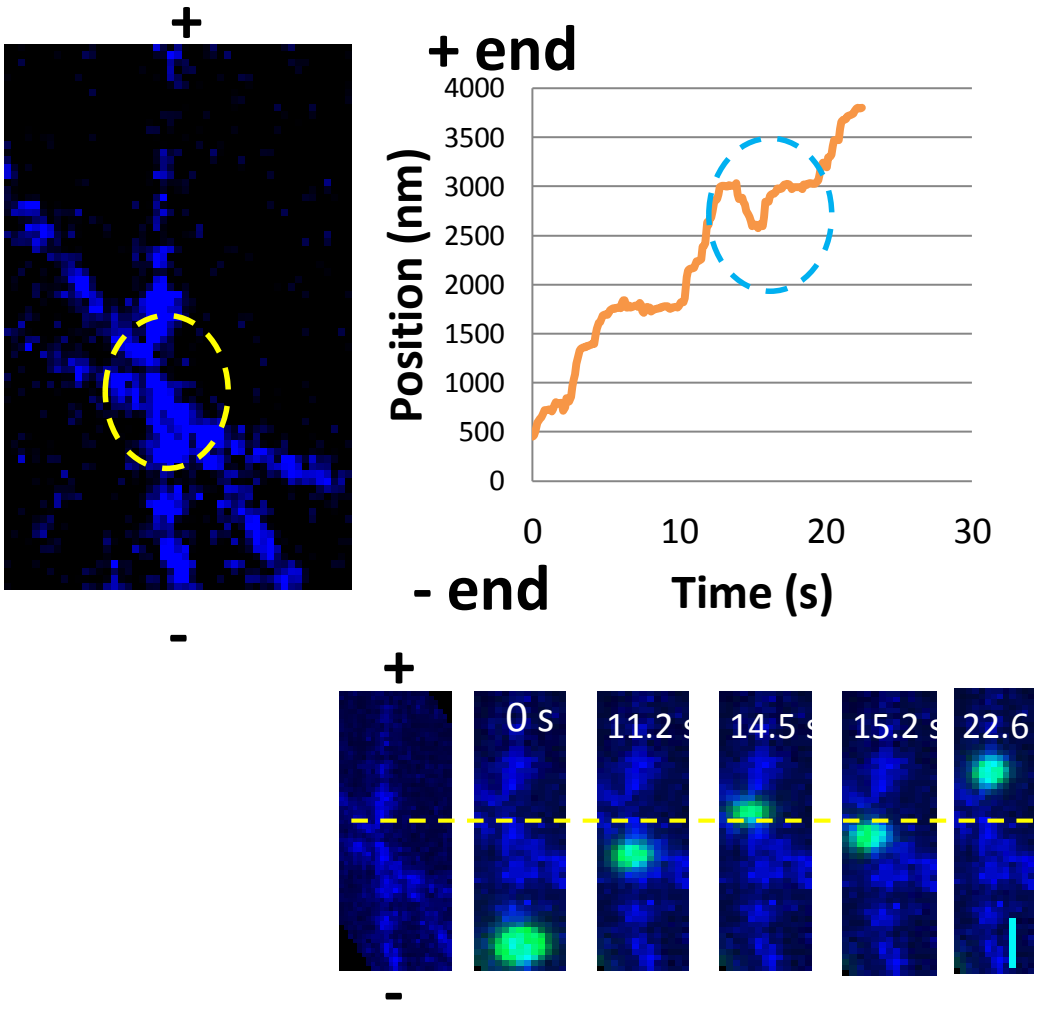

Figure 30. Reversals Allow Successful Bypassing of Microtubule Intersection. A bead bypasses microtubule blockade after reversing directions twice. The microtubules are labeled in blue, with a circle designating the microtubule intersection area. The graph to the right shows the bead hitting the blockade, moving back towards the – end, then repeating the attempt and successfully passing. Select images from the movie. Scalebar =1 µm.

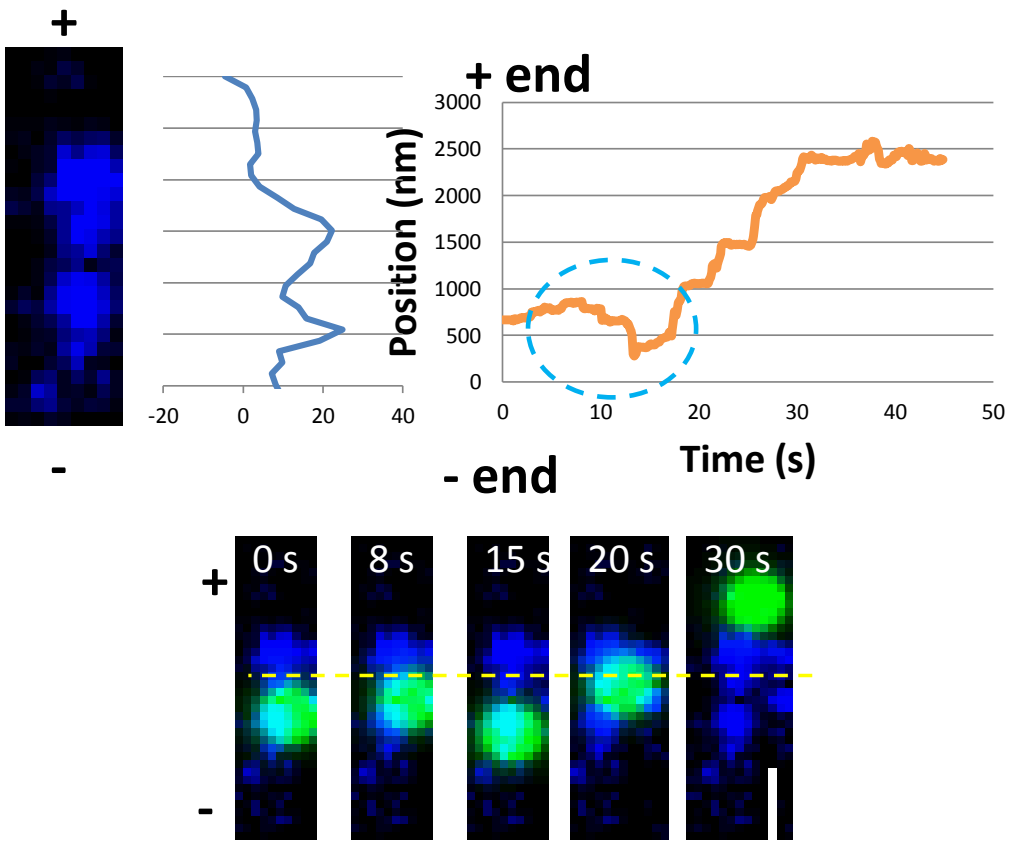

Figure 31. Reversals Allow Successful Bypassing of Tau Protein Obstacle. A bead is able to bypass a patch of tau proteins. Tau proteins are labeled in blue. The graph (right) shows that the bead first moves to the right (the + end) but reverses directions upon encountering the large tau patch. After moving towards the – end, it again reverses and is able to pass the patch on the second try. Select images from the movie. Scalebar =1 µm.

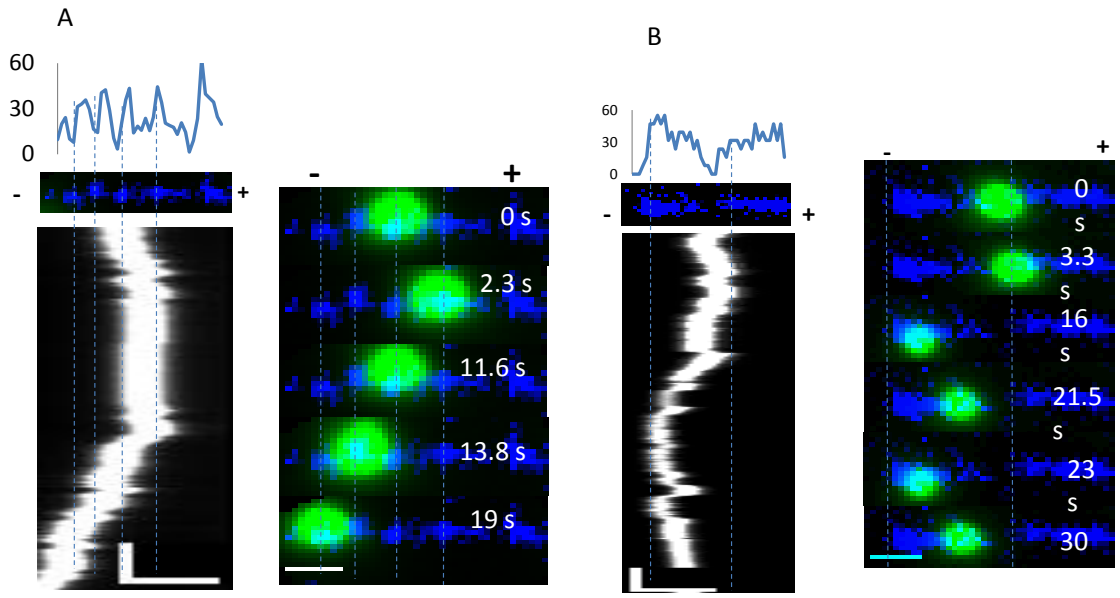

Figure 32. Additonal Examples of Motors Encountering Tau Protein Obstacles. In both cases, the + end of the microtubule is on the right and the – end on the left. Tau proteins are labeled in blue (microtubule are not labeled in this instances). The kymographs below show the movement of the kinesin-and-dynein beads. Scale bars are 2 µm (horizontal) and 2 seconds (vertical). Scalebars for movie images=1 µm. (Left**) A bead bypasses several tau patches after apparently making short, quick reversals at each one. To the right of the kymograph are select images from the movie. (**Right**) A bead is unable to bypass two large patch of tau proteins. The kymograph below shows that the bead appears to be stuck between two large tau patches, hitting one, reversing directions, hitting the other, and reversing again. Select images from the movie are to the right of the kymograph.**

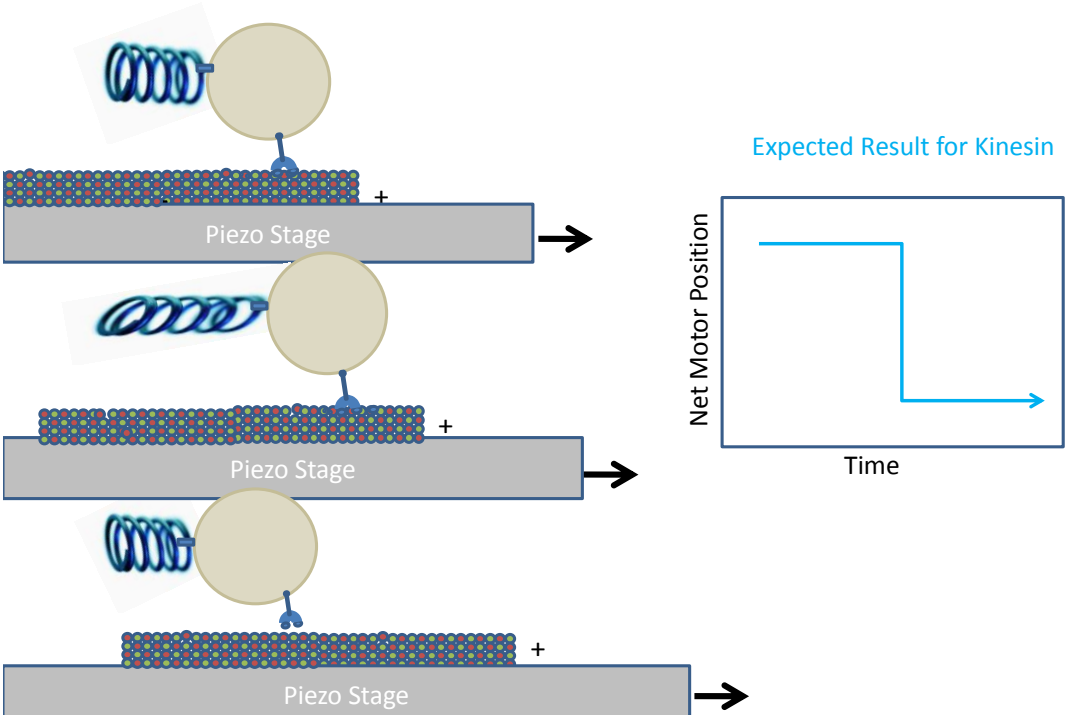

Figure 33. Optical Trap "Snap-back" Experimental Setup. A cartoon depiction illustrating how trap snap-back experiments were conducted. A bead with motors of one type is held in the optical trap and allowed to bind to an microtubule. The piezo stage is then stepped in the direction that the motor would normally walk, which creates a force from the trap in the backwards direction (depicted as a spring in the cartoon). As the "spring" is stretched more and more as the piezo is stepped, the backward force becomes greater and greater until the motor reaches its stall force and releases from the microtubule. At this point, the bead snaps back to the center of the trap, and the motor rebinds. (Right) **A simplified version of the expected graph of net motor motion for a "normal" motor. The motor stays bound as the piezo is stepped but eventually releases and snaps back, causing the net motor position to suddenly jump down.**

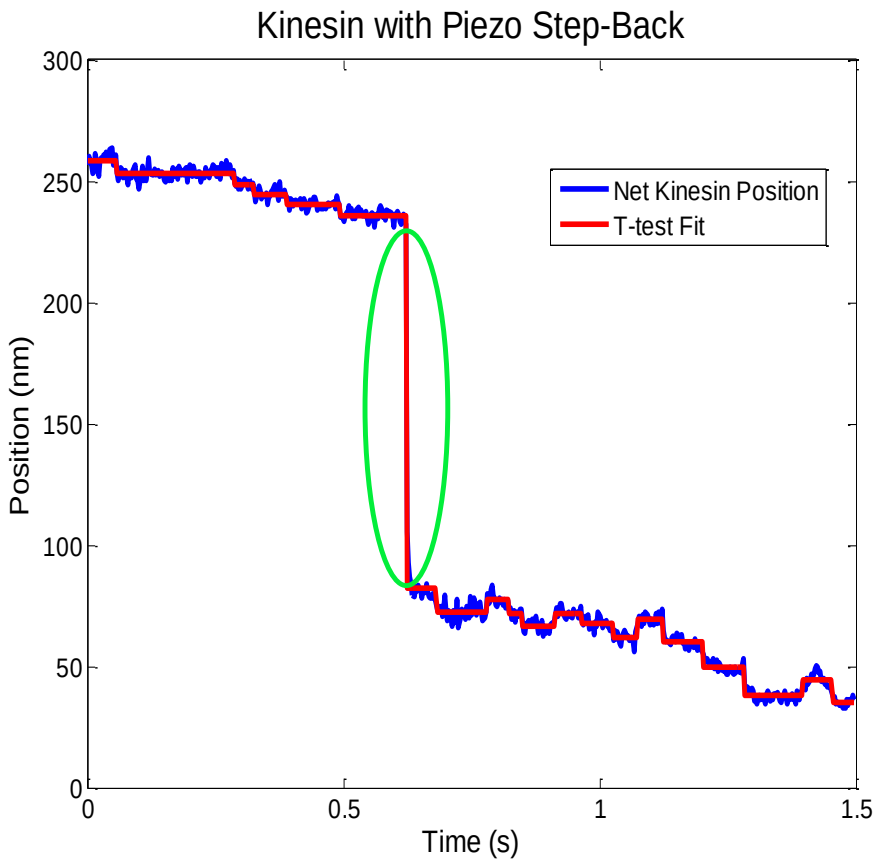

Figure 34. Piezo Step-Back Results for Kinesin-only Beads. Effects of stepping piezo backwards to simulate opposing motors in the optical trap. Net position (bead position in the trap minus the position of the piezo stage as it is stepped back) is in blue. Red line shows the Student T-test fit. The motor's normal direction (i.e. the + end of microtubule for kinesin) is designated as the positive end of the y-axis. The kinesin mostly holds on to the microtubule with a few small backward steps, but then releases from the microtubule as the stall-force is reached, causing the bead to "snap back," as expected.

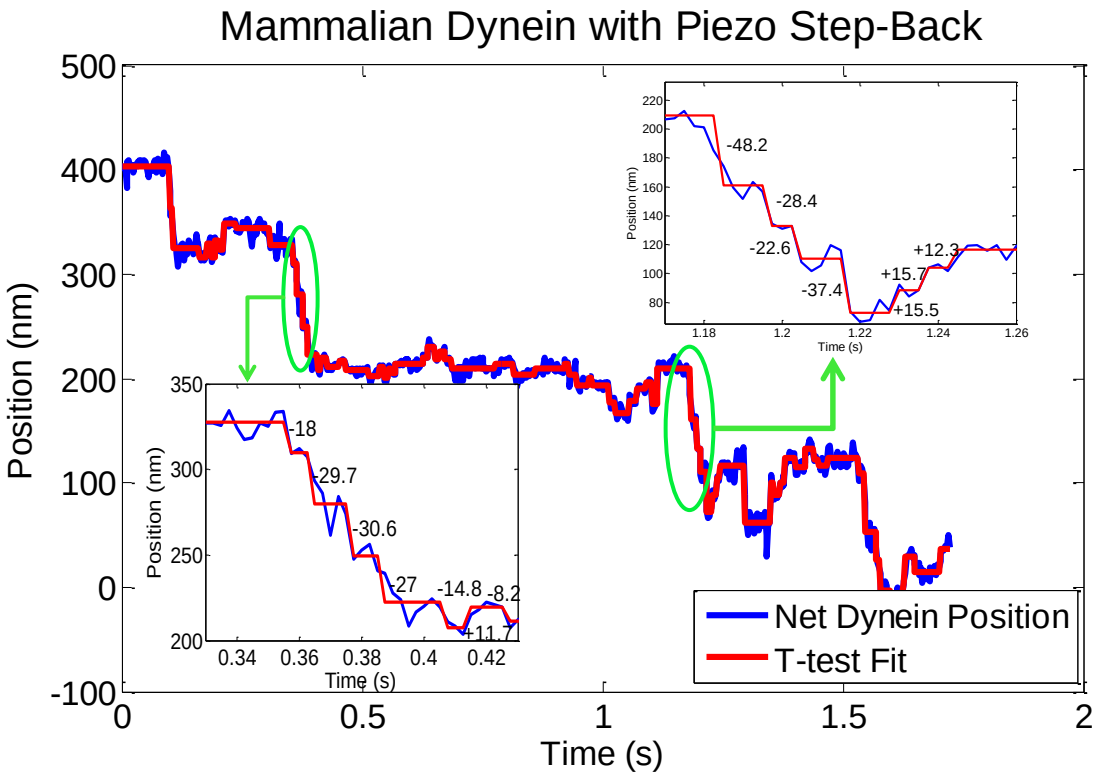

Figure 35. Piezo Step-Back Results for Mammalian Dynein-only Beads. Effects of stepping piezo backwards to simulate opposing motors in the optical trap for beads with mammalian dynein. Net position (bead position in the trap minus the position of the piezo stage as it is stepped back) is in blue. Red line shows the Student T-test fit. The motor's normal direction (i.e. the - end of microtubule for dynein) is designated as the positive end of the y-axis. The trace showing mammalian dynein taking rapid large backwards steps as the piezo is stepped back. The motor does not release from the microtubule but instead rapidly walks backwards. Examples are seen in the green circles (and corresponding zoomed in insets).

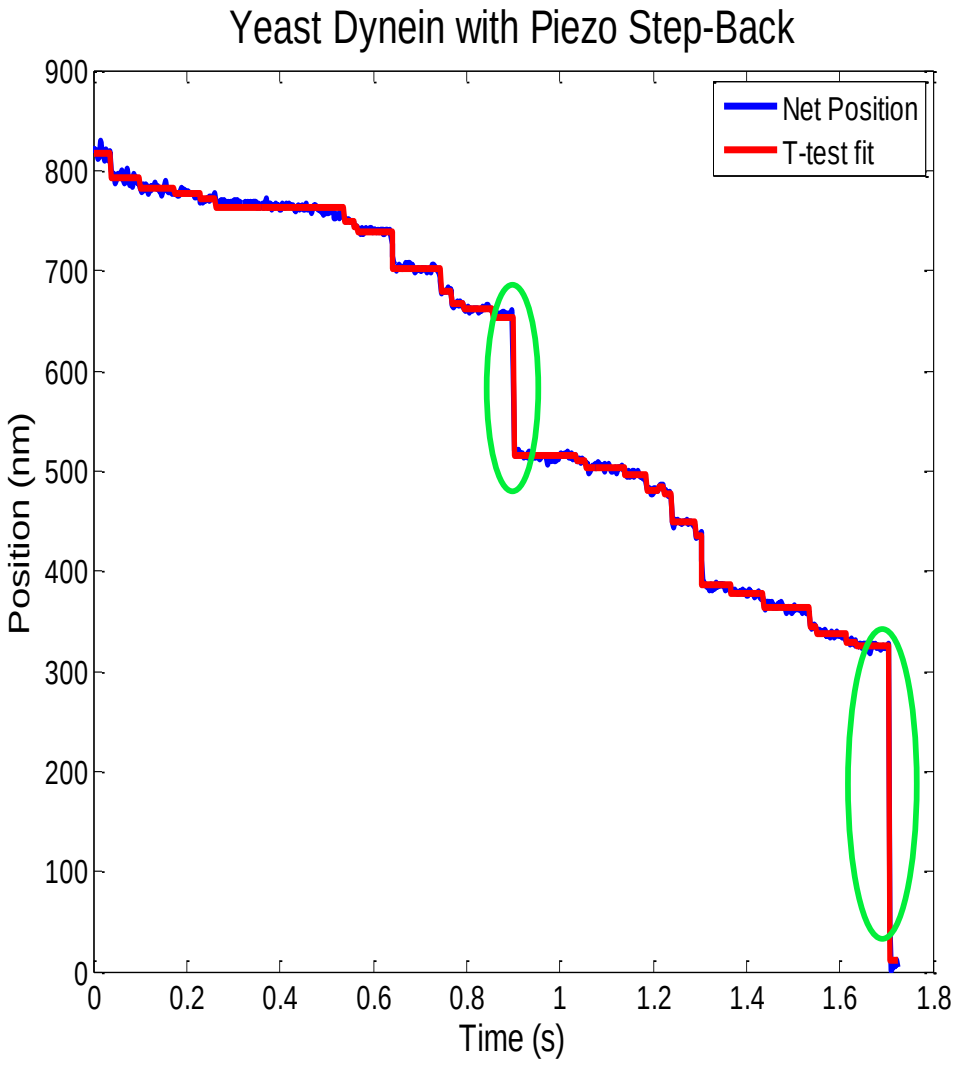

Figure 36. Piezo Step-Back Results for Yeast Dynein-only Beads. Effects of stepping piezo backwards to simulate opposing motors in the optical trap for beads with yeast dynein. Net position (bead position in the trap minus the position of the piezo stage as it is stepped back) is in blue. Red line shows the Student T-test fit. The motor's normal direction (i.e. the - end of microtubule for dynein) is designated as the positive end of the y-axis. A bead with yeast-dynein in place of mammalian-dynein also shows "snap back" behavior. The yeast dynein does take some backwards steps, but mostly holds on to the microtubule tenaciously until snapping back after the stall force is reached, in contrast to mammalian dynein.

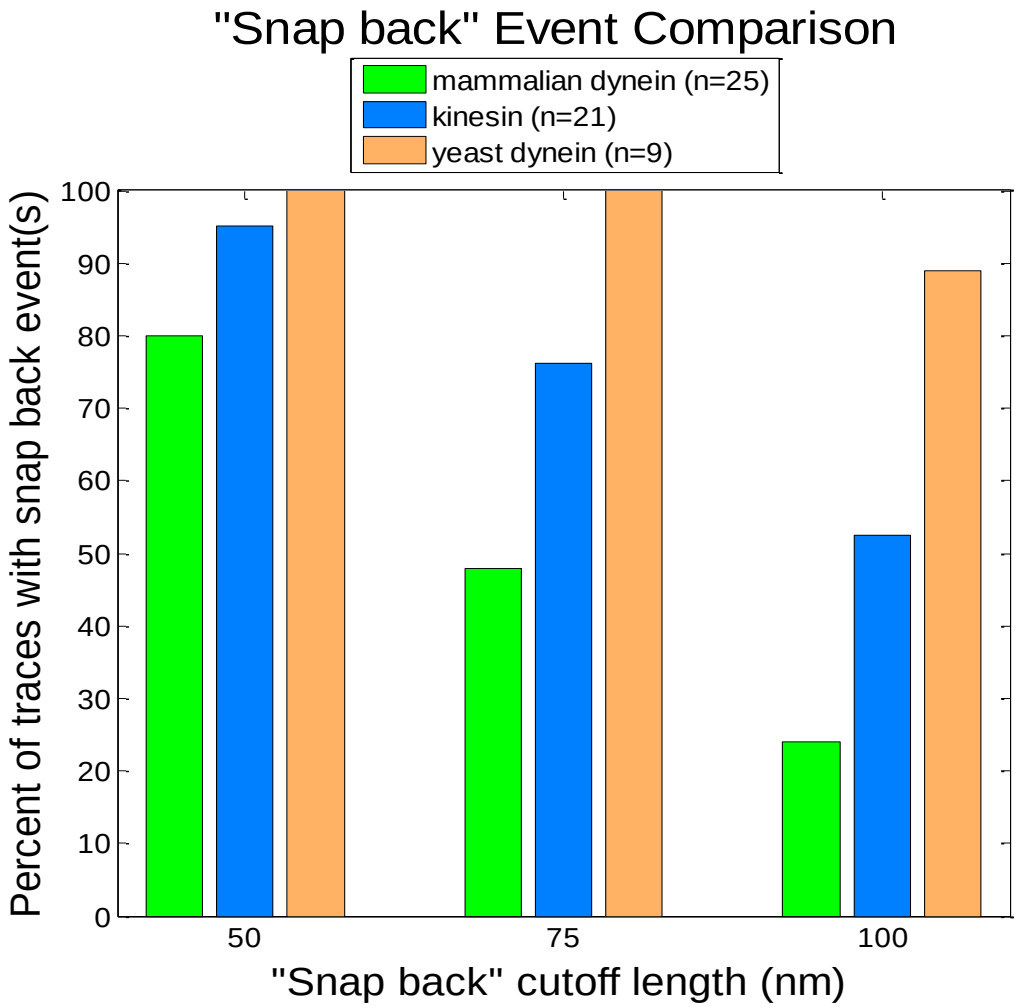

Figure 37. Comparison of "Snap-Back" Events for Kinesin, Mammalian Dynein, and Yeast Dynein. Optical trap traces were fit using Student's T-test. Traces were then scored as having a "snap-back" event if the T-test fit had at least one step with a size larger than a given threshold limit. Threshold limits were set at 50 nm, 75 nm, or 100 nm. (It was assumed that a step of this magnitude indicated a full release from the microtubule rather than an actual motor step.) Mammalian dynein traces showed significantly less snap-back events at all threshold limits, indicating that this motor type was more likely to take backward steps but remain engaged with the microtubule rather than releasing. (See also Figures 34-36.)

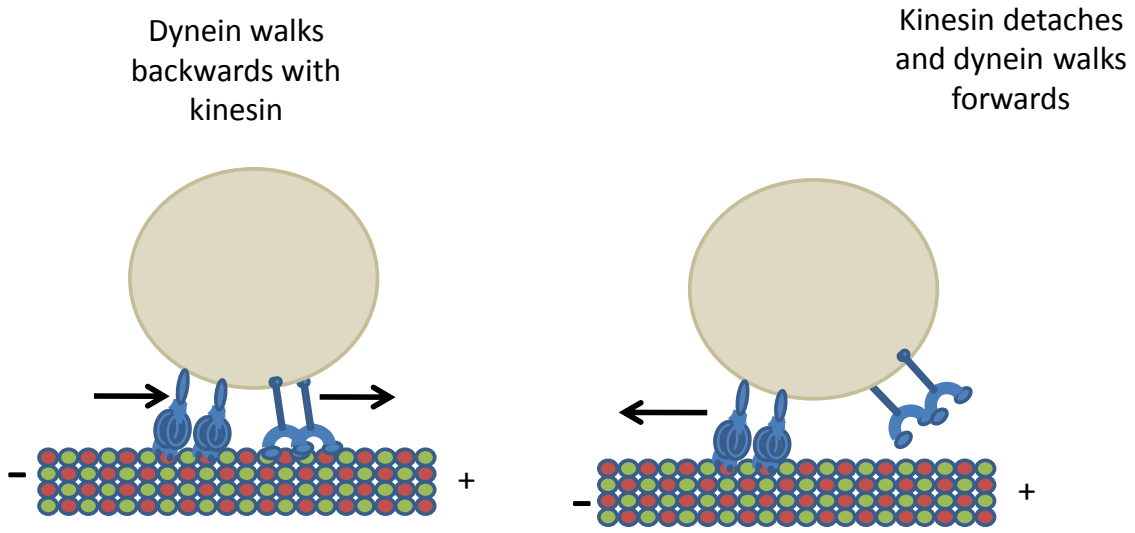

Figure 38. Modified Tug-of-War. A depiction of our hypothesis that dynein does not release from the microtubule while the cargo is moving in the + end direction, but rather walks backwards with kinesin. When kinesin detaches from the microtubule, the dynein takes over and takes the cargo in the – direction.

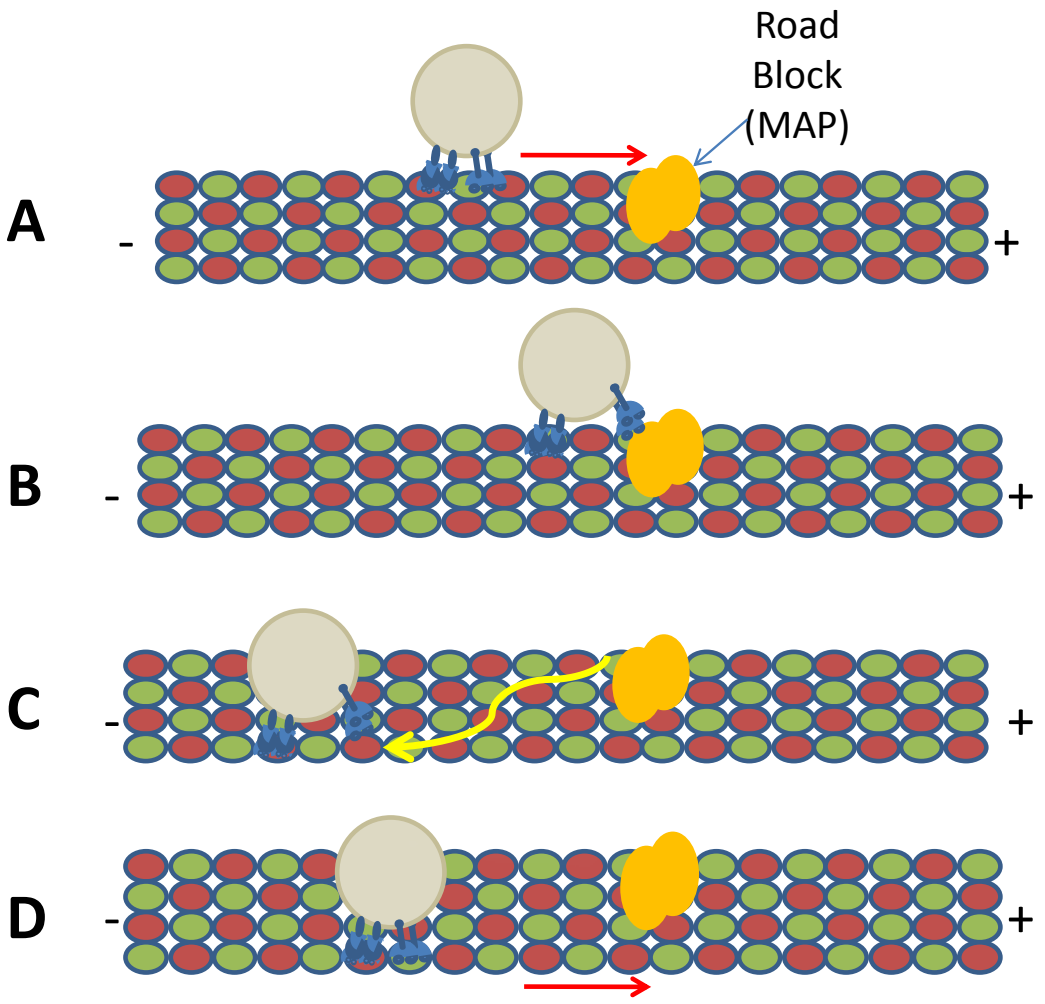

Figure 39. Modified Tug-of-War Model Allows Cargos to Bypass Roadblocks. (A) Kinesin and dynein are both attached to the same cargo. The cargo moves in the + end direction, with kinesin walking forward and dynein walking backwards with kinesin. (B) The cargo encounters a roadblock, such as a microtubule-associated protein (MAP), and the kinesin releases from the microtubule. (C) The dynein is now free to walk in its preferred – end direction. As it does so, it wanders to a new protofilament by taking a few off-axis side steps. (D) The kinesin reattaches to the microtubule, and the cargo starts moving in the + end direction once more. However, it is now able to bypass the roadblock by walking past it on a different protofilament.

References

1. M. B. Elowitz, M. G. Surette, P. Wolf, J. B. Stock, S. Leibler, "Protein Mobility in the Cytoplasm of Escherichia coli," *J. Bacteriol.* **181**, 197 (1999).

2. K. M. Slade, B. L. Steele, G. J. Pielak, N. L. Thompson, "Quantifying Green Fluorescent Protein Diffusion in Escherichia coli by Using Continuous Photobleaching with Evanescent Illumination," *J Phys Chem B* **113**, 4837 (2009).

3. N. Hirokawa, R. Takemura, "Molecular motors in neuronal development, intracellular transport and diseases," *Curr. Opin. Neurobiol.* **14**, 564 (2004).

4. E. Mandelkow, E. Mandelkow, "Tau in Alzheimer's disease," *Trends Cell Biol.* **8**, 425 (1998).

5. R. Dixit, J. R. Ross, Y. E. Goldman, E. L. Holzbaur, "Differential regulation of dynein and kinesin motor proteins by tau," *Science* **319**, 1086 (2008).

6. M. Vershinin, J. Xu, D. S. Razafsky, S. J. King, S. P. Gross, "Multiple-motor based transport and its regulation by Tau," *Proc. Natl. Acad. Sci. U. S. A.* **104**, 87 (2007).

7. S. P. Gilbert, K. A. Johnson, "Expression, purification, and characterization of the Drosophila kinesin motor domain produced in Escherichia coli," *Biochemistry (N. Y.)* **32**, 4677 (1993).

8. A. Yildiz, M. Tomishige, R. D. Vale, P. R. Selvin, "Kinesin Walks Hand-Over-Hand," *Science* **303**, 676 (2004).

9. K. Svoboda, C. F. Schmidt, B. J. Schnapp, S. M. Block, "Direct observation of kinesin stepping by optical trapping interferometry," *Nature* **365**, 721 (1993).

10. W. Hua, E. C. Young, M. L. Fleming, J. Gelles, "Coupling of kinesin steps to ATP hydrolysis," *Nature* **388**, 390 (1997).

11. M. J. Schnitzer, S. M. Block, "Kinesin hydrolyses one ATP per 8-nm step," *Nature* **388**, 386 (1997).

12. D. L. Coy, M. Wagenbach, J. Howard, "Kinesin Takes One 8-nm Step for Each ATP That It Hydrolyzes," *Journal of Biological Chemistry* **274**, 3667 (1999).

13. N. R. Guydosh, S. M. Block, "Backsteps induced by nucleotide analogs suggest the front head of kinesin is gated by strain," *Proc. Natl. Acad. Sci. U. S. A.* **103**, 8054 (2006).

14. Y. Miyazono, M. Hayashi, P. Karagiannis, Y. Harada, H. Tadakuma, "Strain through the neck linker ensures processive runs: a DNA-kinesin hybrid nanomachine study," *EMBO J.* **29**, 93 (2010).

15. E. Toprak, A. Yildiz, M. T. Hoffman, S. S. Rosenfeld, P. R. Selvin, "Why kinesin is so processive," *Proceedings of the National Academy of Sciences*(2009).

16. A. Yildiz, M. Tomishige, A. Gennerich, R. D. Vale, "Intramolecular Strain Coordinates Kinesin Stepping Behavior along Microtubules," *Cell* **134**, 1030 (2008).

17. S. M. Block, "Kinesin motor mechanics: Binding, stepping, tracking, gating, and limping," *Biophys. J.* **92**, 2986 (2007).

18. S. Ray, E. Meyhöfer, R. A. Milligan, J. Howard, "Kinesin follows the microtubule's protofilament axis." *J. Cell Biol.* **121**, 1083 (1993).

19. K. Visscher, M. J. Schnitzer, S. M. Block, "Single kinesin molecules studied with a molecular force clamp," *Nature* **400**, 184 (1999).

20. K. Svoboda, S. M. Block, "Force and velocity measured for single kinesin molecules." *Cell* **77**, 773 (1994).

21. E. Meyhofer, J. Howard, "The Force Generated by a Single Kinesin Molecule Against an Elastic Load," *Proc. Natl. Acad. Sci. U. S. A.* **92**, 574 (1995).

22. N. J. Carter, R. A. Cross, "Mechanics of the kinesin step," *Nature* **435**, 308 (2005).

23. F. J. Kull, E. P. Sablin, R. Lau, R. J. Fletterick, R. D. Vale, "Crystal structure of the kinesin motor domain reveals a structural similarity to myosin," *Nature* **380**, 550 (1996).

24. A. F. Neuwald, L. Aravind, J. L. Spouge, E. V. Koonin, *AAA : A class of chaperone-like ATPases associated with the assembly, operation, and disassembly of protein complexes* .

25. S. R. Gill *et al.*, "Dynactin, a Conserved, Ubiquitously Expressed Component of an Activator of Vesicle Motility Mediated by Cytoplasmic Dynein," *J. Cell Biol.* **115**, pp. 1639 (1991).

26. S. W. Deacon *et al.*, "Dynactin Is Required for Bidirectional Organelle Transport," *J. Cell Biol.* **160**, pp. 297 (2003).

27. S. J. King, T. A. Schroer, "Dynactin increases the processivity of the cytoplasmic dynein motor," *Nat. Cell Biol.* **2**, 20 (2000).

28. T. Culver-Hanlon, S. A. Lex, A. D. Stephens, N. J. Quintyne, S. J. King, "A microtubule-binding domain in dynactin increases dynein processivity by skating along microtubules," *Nat. Cell Biol.* **8**, 264 (2006).

29. J. R. Kardon, S. L. Reck-Peterson, R. D. Vale, "Regulation of the processivity and intracellular localization of Saccharomyces cerevisiae dynein by dynactin," *Proceedings of the National Academy of Sciences*(2009).

30. C. M. Waterman-Storer *et al.*, "The interaction between cytoplasmic dynein and dynactin is required for fast axonal transport," *Proceedings of the National Academy of Sciences* **94**, 12180 (1997).

31. S. Toba, T. M. Watanabe, L. Yamaguchi-Okimoto, Y. Y. Toyoshima, H. Higuchi, "Overlapping hand-over-hand mechanism of single molecular motility of cytoplasmic dynein," *Proceedings of the National Academy of Sciences* **103**, 5741 (2006).

32. S. A. Burgess, M. L. Walker, H. Sakakibara, P. J. Knight, K. Oiwa, "Dynein structure and power stroke," *Nature* **421**, 715 (2003).

33. M. Samsó, M. Radermacher, J. Frank, M. P. Koonce, "Structural characterization of a dynein motor domain," *J. Mol. Biol.* **276**, 927 (1998).

34. C. Cho, S. L. Reck-Peterson, R. D. Vale, "Regulatory ATPase Sites of Cytoplasmic Dynein Affect Processivity and Force Generation," *Journal of Biological Chemistry* **283**, 25839 (2008).

35. T. Kon, T. Mogami, R. Ohkura, M. Nishiura, K. Sutoh, "ATP hydrolysis cycle-dependent tail motions in cytoplasmic dynein," *Nat. Struct. Mol. Biol.* **12**, 513 (2005).

36. T. Kon, M. Nishiura, R. Ohkura, Y. Y. Toyoshima, K. Sutoh, "Distinct Functions of Nucleotide-Binding/Hydrolysis Sites in the Four AAA Modules of Cytoplasmic Dynein," *Biochemistry (N. Y.)* **43**, 11266 (2004).

37. S. L. Reck-Peterson, R. D. Vale, "Molecular dissection of the roles of nucleotide binding and hydrolysis in dynein's AAA domains in Saccharomyces cerevisiae," *Proceedings of the National Academy of Sciences of the United States of America* **101**, 1491 (2004).

38. I. R. Gibbons, A. J. Rowe, "Dynein: A Protein with Adenosine Triphosphatase Activity from Cilia," *Science* **149**, 424 (1965).

39. I. R. Gibbons, "STUDIES ON THE PROTEIN COMPONENTS OF CILIA FROM TETRAHYMENA PYRIFORMIS," *Proceedings of the National Academy of Sciences* **50**, 1002 (1963).

40. B. M. Paschal, R. B. Vallee, "Retrograde transport by the microtubule-associated protein MAP 1C," *Nature* **330**, 181 (1987).

41. R. Mallik, B. C. Carter, S. A. Lex, S. J. King, S. P. Gross, "Cytoplasmic dynein functions as a gear in response to load," *Nature* **427**, 649 (2004).

42. A. Gennerich, A. P. Carter, S. L. Reck-Peterson, R. D. Vale, "Force-Induced Bidirectional Stepping of Cytoplasmic Dynein," *Cell* **131**, 952 (2007).

43. R. Mallik, D. Petrov, S. A. Lex, S. J. King, S. P. Gross, "Building Complexity: An In Vitro Study of Cytoplasmic Dynein with In Vivo Implications," *Curr. Biol.* **15**, 2075 (2005).

44. J. L. Ross, K. Wallace, H. Shuman, Y. E. Goldman, E. L. F. Holzbaur, "Processive bidirectional motion of dynein-dynactin complexes in vitro," *Nat. Cell Biol.* **8**, 562 (2006).

45. Z. Wang, M. P. Sheetz, "One-dimensional diffusion on microtubules of particles coated with cytoplasmic dynein and immunoglobulins," *Cell Struct. Funct.* **24**, 373 (1999).

46. M. Miura, A. Matsubara, T. Kobayashi, M. Edamatsu, Y. Y. Toyoshima, "Nucleotide-dependent behavior of single molecules of cytoplasmic dynein on microtubules in vitro," *FEBS Lett.* **584**, 2351 (2010).

47. S. Reck-Peterson *et al.*, "Single-Molecule Analysis of Dynein Processivity and Stepping Behavior," *Cell* **126**, 335 (2006).

48. Z. Wang, S. Khan, M. P. Sheetz, "Single cytoplasmic dynein molecule movements: characterization and comparison with kinesin," *Biophys. J.* **69**, 2011 (1995).

49. R. B. Vallee, J. C. Williams, D. Varma, L. E. Barnhart, "Dynein: An ancient motor protein involved in multiple modes of transport," *J. Neurobiol.* **58**, 189 (2004).

50. L. I. Rebhun, "Structural aspects of saltatory particle movement," *J. Gen. Physiol.* **50**, 223 (1967).

51. S. Klumpp, R. Lipowsky, "Active diffusion of motor particles," *Phys. Rev. Lett.* **95**(2005).

52. M. A. Welte, "Bidirectional Transport along Microtubules," *Current Biology* **14**, R525 (2004).

53. V. Muresan, C. P. Godek, T. S. Reese, B. J. Schnapp, "Plus-end motors override minus-end motors during transport of squid axon vesicles on microtubules." *The Journal of Cell Biology* **135**, 383 (1996).

54. S. P. Gross, M. A. Welte, S. M. Block, E. F. Wieschaus, "Coordination of Opposite-Polarity Microtubule Motors," *J. Cell Biol.* **156**, pp. 715 (2002).

55. A. Uchida, N. H. Alami, A. Brown, "Tight functional coupling of kinesin-1A and dynein motors in the bidirectional transport of neurofilaments," *Mol. Biol. Cell* **20**, 4997 (2009).

56. M. Martin *et al.*, "Cytoplasmic dynein, the dynactin complex, and kinesin are interdependent and essential for fast axonal transport." *Mol. Biol. Cell* **10**, 3717 (1999).

57. S. Ling, P. S. Fahrner, W. T. Greenough, V. I. Gelfand, "Transport of Drosophila fragile X mental retardation protein-containing ribonucleoprotein granules by kinesin-1 and cytoplasmic dynein," *Proc. Natl. Acad. Sci. U. S. A.* **101**, 17428 (2004).

58. A. D. Pilling, D. Horiuchi, C. M. Lively, W. M. Saxton, "Kinesin-1 and Dynein Are the Primary Motors for Fast Transport of Mitochondria in Drosophila Motor Axons," *Mol. Biol. Cell* **17**, 2057 (2006).

59. C. Kural *et al.*, "Kinesin and Dynein Move a Peroxisome in Vivo: A Tug-of-War or Coordinated Movement?" *Science* **308**, 1469 (2005).

60. V. Levi, A. S. Serpinskaya, E. Gratton, V. Gelfand, "Organelle Transport along Microtubules in Xenopus Melanophores: Evidence for Cooperation between Multiple Motors," *Biophys. J.* **90**, 318 (2006).

61. J. A. Laib, J. A. Marin, R. A. Bloodgood, W. H. Guilford, "The reciprocal coordination and mechanics of molecular motors in living cells," *Proceedings of the National Academy of Sciences*(2009).

62. M. J. I. Müller, S. Klumpp, R. Lipowsky, "Tug-of-war as a cooperative mechanism for bidirectional cargo transport by molecular motors," *Proceedings of the National Academy of Sciences* **105**, 4609 (2008).

63. R. D. Vale, F. Malik, D. Brown, "Directional instability of microtubule transport in the presence of kinesin and dynein, two opposite polarity motor proteins." *J. Cell Biol.* **119**, 1589 (1992).

64. S. Ally, A. G. Larson, K. Barlan, S. E. Rice, V. I. Gelfand, "Opposite-polarity motors activate one another to trigger cargo transport in live cells," *The Journal of Cell Biology* **187**, 1071 (2009).

65. V. Soppina, A. K. Rai, A. J. Ramaiya, P. Barak, R. Mallik, "Tug-of-war between dissimilar teams of microtubule motors regulates transport and fission of endosomes," *Proceedings of the National Academy of Sciences* **106**, 19381 (2009).

66. A. G. Hendricks *et al.*, "Motor Coordination via a Tug-of-War Mechanism Drives Bidirectional Vesicle Transport," *Current Biology* **20**, 697 (2010).

67. M. Schuster, R. Lipowsky, M. Assmann, P. Lenz, G. Steinberg, "Transient binding of dynein controls bidirectional long-range motility of early endosomes," *Proc. Natl. Acad. Sci. U. S. A.* **108**, 3618 (2011).

68. T. Fallesen, J. Macosko, G. Holzwarth, "Force–velocity relationship for multiple kinesin motors pulling a magnetic bead," *European Biophysics Journal*, 1 (2011).

69. A. Yildiz *et al.*, "Myosin V Walks Hand-Over-Hand: Single Fluorophore Imaging with 1.5-nm Localization," *Science* **300**, 2061 (2003).

70. S. M. Block, L. S. Goldstein, B. J. Schnapp, "Bead movement by single kinesin molecules studied with optical tweezers," *Nature* **348**, 348 (1990).

71. H. Lu, Y. Ali, c. S. Bookwalter, D. M. Warshaw, K. M. Trybus, "Diffusive Movement of Processive Kinesin-1 on Microtubules," *Traffic* **10**, 1429 (2009).

72. D. W. Pierce, R. D. Vale, "Assaying processive movement of kinesin by fluorescence microscopy." *Meth. Enzymol.* **298**, 154 (1998).

73. J. B. Bingham, S. J. King, T. A. Schroer, in Methods in Enzymology, Richard B. Valee, Ed. (Academic Press, , 1998), pp. 171-184, vol. Volume 298.

74. S. Kar, J. Fan, M. J. Smith, M. Goedert, L. A. Amos, "Repeat motifs of tau bind to the insides of microtubules in the absence of taxol," *EMBO J.* **22**, 70 (2003).

75. N. M. Green, "Avidin," *Adv. Protein Chem.* **29**, 85 (1975).

76. T. Courtheoux *et al.*, "Dynein participates in chromosome segregation in fission yeast," *Biology of the Cell* **99**, 627 (2007).

77. N. J. Carter, R. A. Cross, "Mechanics of the kinesin step," *Nature* **435**, 308 (2005).

78. M. Nishiyama, H. Higuchi, T. Yanagida, "Chemomechanical coupling of the forward and backward steps of single kinesin molecules," *Nat. Cell Biol.* **4**, 790 (2002).

79. H. Li, D. J. DeRosier, W. V. Nicholson, E. Nogales, K. H. Downing, "Microtubule Structure at 8 Å Resolution," *Structure* **10**, 1317 (2002).

80. R. D. Vale, "The Molecular Motor Toolbox for Intracellular Transport," *Cell* **112**, 467 (2003).

Appendix: Details of Analysis Program

Section A1: Making the Microtubule Mask

1. A movie is read in which shows the fluorescent microtubules. The program averages the frames together to get rid of some noise, then thresholds the image to give a black and white picture of the brightest areas (which are the microtubules, plus some noise). The user is given the option to select microtubule areas which were missed. It then looks for areas of white pixels that are adjoining and have a large enough area and throws out the smaller (just background noise) areas. It labels each of the remaining white areas, and then fits them to lines.

2. The microtubule lines are made into a rectangle of arbitrary height (in this case, 15 pixels) and the length of the microtubules. It saves the endpoint of each rectangle along with the angle it makes with the horizontal.

3. A "mask" is created that can be applied to other movies. This is an image that is 0 (black) everywhere except where the microtubule rectangles are, where it is 1 (white). If this mask is multiplied by an image in the data file, it "erases" spots that are not located on the microtubules.

4. A movie of labeled truncated kinesin walking on the microtubules is then read in. This is used to determine the directionality of the microtubules (+/- ends). First the reference kinesin movie is summed up using the standard deviation method (the standard deviation of each pixel is determined over time and then that value is saved

in that pixel position in the final summed image.) This effectively shows where the kinesins are walking (the moving spots have a higher standard deviation, so lines of moving kinesin are produced). Then the same line-finding method that was previously used on the microtubule image is used to find the lines of moving kinesins in this movie.

5. The lines of the reference kinesin movie are matched up with the lines of the microtubules (the differences between the images are minimized) to line up the two images and determine the offset of the microtubule image. (This is necessary because a slide-in filter used to image the microtubules creates a significant--but not consistent--offset between the two colors of images).

Section A2: Kymographs (determining microtubule polarity)

6. The offset-corrected mask is now applied to the full reference kinesin movie. Each microtubule is taken individually, excised from the movie, and rotated by the angle saved earlier to make it perfectly horizontal. Then a kymograph is created by summing the intensity of each x position on the microtubule versus time. This shows "tracks" of where the reference kinesin traveled. The program then fits lines to the tracks and determines the slope to figure out which was the + direciton of the microtubule. It sets the polarity to 0 if it is ambiguous or has traces going both ways. (Manual input is requested to check the polarity assignment of these kymographs.)

7. The polarity of each microtubule is then saved along with the angle and end positions found earlier.

Section A3: Finding Moving Spots

8. Next, the "real data" movie is read in and the mask is applied to it. The movie is then normalized through time (the intensity of each pixel over time is summed up and then the pixel at a given frame is divided by that intensity). This serves to eliminate (or at least reduce) any spots that are not moving, while preserving the moving spots.

9. The normalized image is then threshholded (spots more than five times the standard deviation of the background are kept).

10. The program then looks at the image as a 3-d matrix and finds 3-d volumes of contiguous 1's (white areas) that are greater than the threshold volume. It also throws out volumes that don't meet certain criteria (i.e., the path-length along the microtubule is too short).

11. Each remaining volume is then "excised" from the stack and the corresponding area over the corresponding frames is excised from the original data movie.

12. The excised movie is rotated by the angle of the microtubules (with the + end always on the right) so that the microtubule direction is horizontal.

13. The centroid of the spot is determined as a rough estimate of the position. The y variance of the centroid is determined for each frame. This is used to determine if the bead is merely floating around or actually attached to the microtubule. (Floating beads have a large y variance while attached ones have a much smaller variance.) If the variance is too large over the whole movie, it is thrown out. If it has a "good" section, this is trimmed out with the large variance sections cut off from the beginning/end. The remaining movie is then written to a tiff file.

14. Matlab calls a command-line version of IDL (an image processing programming language) to run the FIONA fitting routine typically used in our lab for FIONA analysis (based on "Simonsin_simple_FIONA"). This is "wrapped" in a Matlab function so that it can be called without leaving Matlab. IDL is used because its 2-D Gaussian fitting function is vastly superior to Matlab's.

15. The positions and errors as determined by FIONA are saved for each trace (and written to an excel file). The program looks for errors above a given cutoff (can be set by user) and sets the corresponding positions to NaN. If the NaN section is short (less than 6 frames), it interpolates to find the values instead. If it is larger than 5 frames, it simply ignores that section for the rest of the analysis.

Section A4: Finding Reversals

16. Using the Recursive Douglas-Peucker Polyline Simplification algorithm, it finds segments of roughly constant velocity and generates histograms of various measures

such as segment lengths, velocities, etc. Net distance traveled and ratio of net distance to total pathlength is also calculated. Traces with a net distance of less than 50 nm are thrown out.

17. Locates places where the beads reversed direction by looking for places where the slope changes sign with some minimum distance traveled (ie, 250 nm) on either side of the slope change. Values such as the average distance and time between reversals are recorded in a spreadsheet.

18. The traces are plotted in Powerpoint, and the excised movies are screened manually to ensure the plotted trace reflects the actual movement in the movie, and to exclude movies with multiple moving beads or other error-inducing issues.

19. Traces from experiments with identical conditions are grouped and the statistics from the traces are compiled.